Mathematically Modelling Multilayer Structures and Reflective Surfaces to Predict and Explain the Optical Properties of Iridescent Elytra

Andrew Nicoll

July 2, 2018

Abstract

This paper presents ways of mathematically modelling the structural colour and reflective properties of multilayer structures as seen naturally occurring in some beetle elytra (hardened forewings). This was achieved by writing code that incorporates some of the relevant mathematics of computational electrodynamics, such as the transfer matrix method, in conjunction with original models for relative reflected intensities and wavelength. Spectral data was collected from elytra using an optical spectrometer and goniometer, and transmission electron microscopy (TEM) provided accurate dimensions of individual layers in the multilayer structure. Overall, the models showed to be accurate in approximating and predicting the patterns in data for non-treated elytra as well as water treated elytra. Furthermore, the average predicted layer thicknesses for non-treated and water treated elytra were 110nm and 105nm respectively. In addition, experiments and modelling complied with the hypothesis on changing spectral bandwidth, but a full conclusion to whether the hypothesis is true has not been established.

Contents

Introduction

Unlike "normal" colour which is a result of pigments present in a material, structural colour such as iridescence is caused by nanoscale objects including thin-films and multilayer reflectors, which are also referred to as one dimensional photonic crystals. In nature, iridescence caused by multilayer structures is often present in beetles such as the *Chrysochroa wallacei,* which is the focus of investigation in this paper.

The process of mathematical modelling is to set up a system of equations that try and describe as effectively as possible the results of an experiment. This allows one to predict the outcome of an experiment with certainty by understating how the system changes. The optical physics of multilayer structures have been explained thoroughly in many academic papers [1-6]. However, this paper explores a slightly different approach where the aim is to use similar mathematics and original models to not only investigate the properties of structural colour in elytra but also to model the relative reflected intensities of surfaces and reflectance of multilayers as well as single dielectric interfaces. This allows for a more specific and complete representation of the various optical aspects of elytra which aided the prediction and description of key patterns and characteristics in spectral data obtained from non-treated and water treated elytra with reasonable accuracy.

Furthermore, using TEM allowed layer thickness's and the number of layers in the multilayer reflector to be measured very accurately, which were then used to compare the results of the models concerning iridescence. Moreover, the change in spectral bandwidth with changing angle of incidence and viewing angle was investigated which appears to be unprecedented. All the modelling was achieved by independently writing original computer code in Python.

The first chapter of this paper intends to provide an overview of the physical mechanisms of iridescence in multilayer reflectors and applying the theory to the structural colour of elytra. The next part of the chapter looks at wavelength data obtained from non-treated and water treated elytra and predicting it with the relevant mathematics. The second chapter focuses on relative reflected intensities for curved surfaces which are dealt with an original model involving mathematical ideas that have not been applied in this context before. The third chapter looks at producing modelled spectra which incorporates the mathematics from previous chapters in conjunction with a curve fitting technique called Lagrange Interpolation. Chapter 4 looks briefly at computational electrodynamics including Maxwell's equations, the Fresnel equations and the transfer matrix method. This theory is then applied to models for reflectance, and then it is later compared to experimental data. We finish the paper by investigating the hypothesis on changing spectral bandwidth in chapter 5.

Chapter 1: Modelling Iridescence

1.1 Structural colour and iridescence

Structural colour is often produced by nanostructures interfering with light as opposed to pigments. Iridescence is a property exhibited by these surfaces and is defined as the gradual change of reflected colour as the angle of illumination or angle of view changes [7]. The term "colour" in this case refers to electromagnetic waves with a range of wavelengths[1] between 390-700 nm that make up visible light. To understand and mathematically model colour changes involved in iridescence, we must first look at thin films and multilayer reflectors which are responsible for the optical mechanisms that cause iridescence.

1.2 Thin film interference

When light hits a surface, it can either be reflected, transmitted or absorbed. If at this interface there is change in refractive index, then light is reflected. A thin film involves a thin layer of material that allows for light to be reflected or transmitted at its upper and lower boundaries [8].

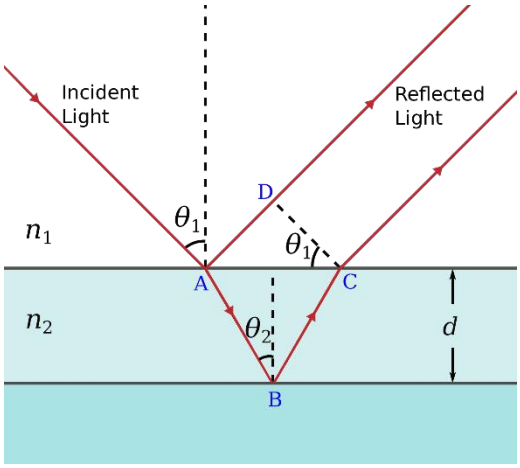

Figure 1.1: *Demonstration of the behaviour of light in a thin film [8]*

In figure 1.1, some of the incident light is reflected and refracted at point *A*. The refracted light passes through the second material and is reflected from the lower boundary at *B* and once again is refracted at *C* as it enters the initial entrance medium. This results in two separate rays of light which we will see later can interfere and bring about specific colours resulting in iridescence.

1.2.1 Refraction

Refraction is the change in direction of propagation of light as it travels from a medium of a given refractive index into another medium of a different refractive index. The absolute refractive index, *n*, is the property of a material that describes how light propagates through it. It is given by the equation,

$$n = \frac{c}{v},$$

[1] The wavelength of a wave is the distance between two adjacent troughs or two adjacent peaks

where v is the velocity of light in the given material and c is the speed of light in a vacuum.

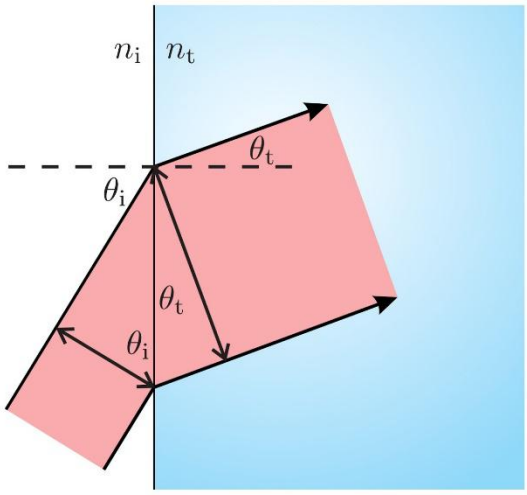

Figure 1.2: *Refraction of light at an interface [9]*

In figure 1.2, n_i and n_t are the refractive indices of the entrance and exit mediums respectively. The incident light hits the surface of the material at an angle of incidence θ_i which is the angle between the normal of the surface and the direction of incident light. At the interface, the light is refracted and changes direction which is measured by the angle of refraction, θ_t. The relationship between refractive index and angle is given by Snell's Law,

$$n_i \sin\theta_i = n_t \sin\theta_t.$$

Total internal reflection is the complete reflection of light off an interface such as the one in figure 1.2 and occurs when the angle of incidence is greater than the critical angle of the transmitting material. In figure 1.1, the refraction of light in the thin film occurs at points A and C as light enters and exits the second medium and total internal reflection occurs at point B.

1.2.2 Interference

From figure 1.1, it is clear to see the ray of light emerging at C has travelled a greater distance from A than the reflected ray due to the thickness d of the thin film. These two waves eventually re-join. However, the extra distance travelled in the thin film, as well as the refractive indices, will determine the phase difference between the two exiting rays. The phase of a wave describes the fraction of a cycle completed compared to the start of the cycle. Particles in parts of a wave that are moving at the same speed and direction are in phase. Particles in phase are separated by a whole number, n, of wavelengths, $n\lambda$ [10]. They are out of phase if they are at different points in their cycle at a particular time. As light reflects off a denser medium ($n_t > n_i$) the wave will undergo a phase change of half a cycle (180°). This happens at point A in figure 1.1.

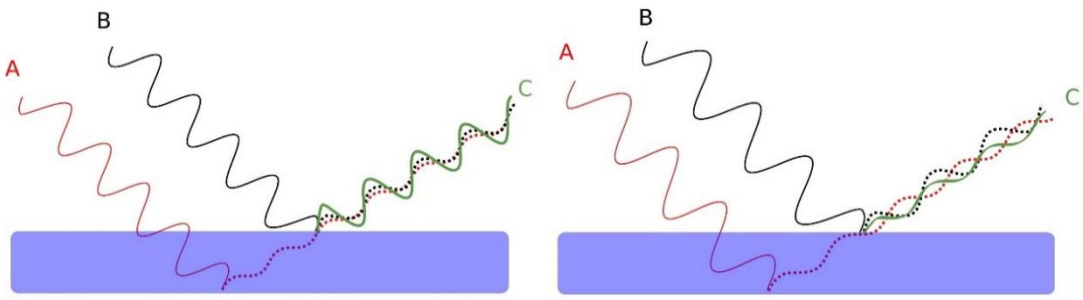

Figure 1.3: *Constructive interference (left) and destructive interference (right) [8]*

As shown in figure 1.3 (left), if the two waves *A* and *B* emerging from the surface are in phase then constructive interference occurs and produces a wave, *C*, with larger amplitude. If the emerging waves are out of phase (right), then *C* has a lower amplitude. Therefore, bright reflected light will be observed when constructive interference takes place [8].

The distance travelled by the refracted ray in the film will depend upon the angle of incidence, refractive indices and the thickness of the thin film. The condition for constructive interference can be related to the optical path difference which is given by,

$$2n_2 d\cos\theta_2.$$

Interference will be constructive if the optical path difference is equal to an integer multiple of the wavelength λ [5], where *m* is an integer,

$$m\lambda = 2n_2 d\cos\theta_2.$$

If the full spectrum of colours in white light is incident, then for a given film thickness and refractive index only certain wavelengths will satisfy the condition of constructive interference. In other words, only selected colours will be strongly reflected at a particular angle of incidence and thus will have a dominant reflection peak. If the film is thin enough, only one colour will be reflected at a given angle. This is the concept of iridescence, where particular colours of light are visible at different angles of incidence or view.

1.3 Multilayer reflectors

A multilayer structure is based upon a thin film system as it is comprised of multiple alternating parallel layers of two different materials with differing refractive indices [1] (figure 1.4). Such a structure behaves as a reflector when the optical thickness of all the layers are comparable to the wavelength of incident light.

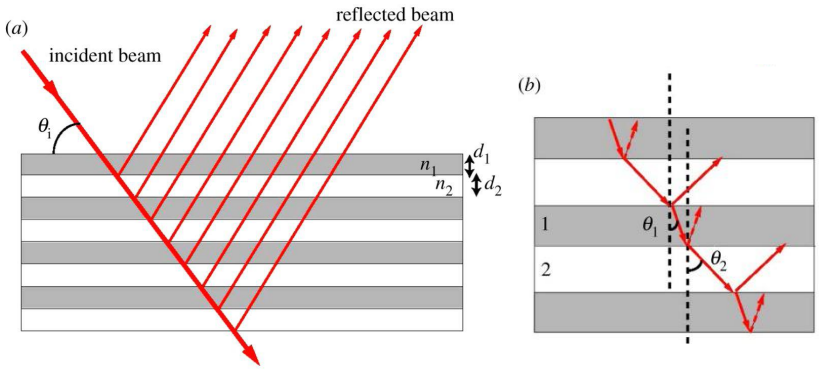

Figure 1.4: *Demonstration of the behaviour of light in a multilayer reflector, general cross section of a multilayer (a) and refraction and reflection between the layers (b) [11]*

Due to the extra layers, even stronger constructive interference could occur in a multilayer reflector compared to a thin film resulting in stronger and purer colours. The condition for constructive interference for a multilayer is similar to that of a thin film. Since a multilayer can be represented as a stack of thin films then the equation for constructive interference is simply the sum of the optical path differences in the two materials [1],

$$\lambda_{\max} = 2(n_1 d_1 \cos\theta_1 + n_2 d_2 \cos\theta_2),$$

where λ_{max} is the dominant reflected wavelength and $\theta_1 \neq 0$. This can also be written in terms of the medium light is incident from, n_0, [5],

$$m\lambda = 2\left(d_1\sqrt{n_1^2 - n_0^2\sin^2\theta_0} + d_2\sqrt{n_2^2 - n_0^2\sin^2\theta_0}\right), \qquad (1)$$

where θ_0 is the angle of incidence in the entrance medium RI=n_0. When the optical thickness, *nd*, of both layers are equal, the system is referred to as an *ideal* multilayer [1]. When $\theta_0=0$, the interference condition reduces to,

$$\frac{\lambda}{4} = n_1 d_1 = n_2 d_2.$$

1.4 Multilayer structures in elytra

An elytron (*pl*: elytra) is the hardened forewing of a beetle. Images of elytra are found on page 52. In some species, multilayer structures can be found on the upper surface of the elytra resulting in the beetle exhibiting iridescent properties. Generally, these naturally occurring structures consist of a stack of around 20 layers and in insects the main layer is almost always chitin[2] with the other layer often being air or melanin. The iridescent beetle investigated in this project was the *Chrysochroa wallacei* which was mainly considered to have a multilayer structure

[2] Chitin is a naturally occurring material found in insects

with alternating layers of chitin and air. The dimensions of the multilayers were examined in detail using transmission electron microscopy.

1.4.1 TEM

Transmission electron microscopy (TEM) is a technique where a high energy beam of electrons is shone through a very thin sample. The interaction of the electrons and the atoms in the sample allow clear black and white images of nanostructures to be observed in the specimen. In this case, the technique proved to be vital in the mathematical modelling of iridescence since the dimensions of the multilayer structures in the *C. wallacei* elytra would be known accurately.

1.4.1.1 Imaging

Figure 1.5 shows the multilayer reflector in a non-treated elytron consisting of 19 layers of chitin (darker layers) and lighter air layers. The multilayer showed to be located on the top surface of an elytron.

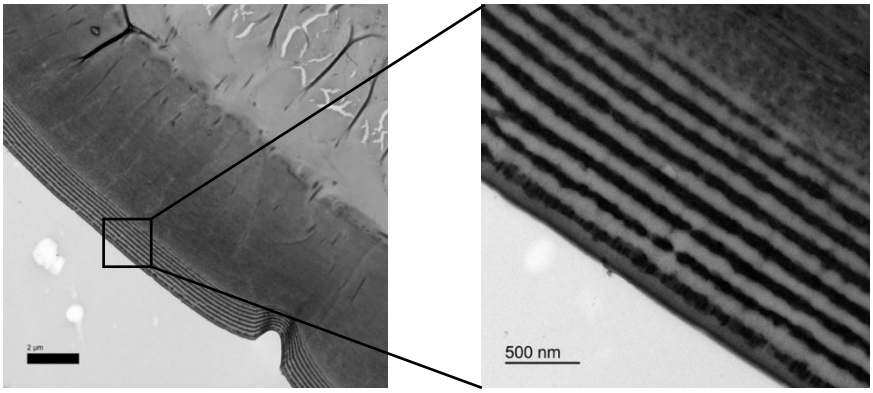

Figure 1.5: *Multilayer stack consisting of 19 layers, 18,000 magnification (left) and 25,000 magnification (right).*

The analysis of these images enabled the individual layer thicknesses to be calculated (figure 1.6) as well as the total number of layers. It was concluded from multiple imaging that the layer thicknesses of chitin and air were consistently similar throughout the multilayer structure. A single layer varied in size from around 80-100 nm, with the thickness of both layers 1 and 2 averaging around 100nm.

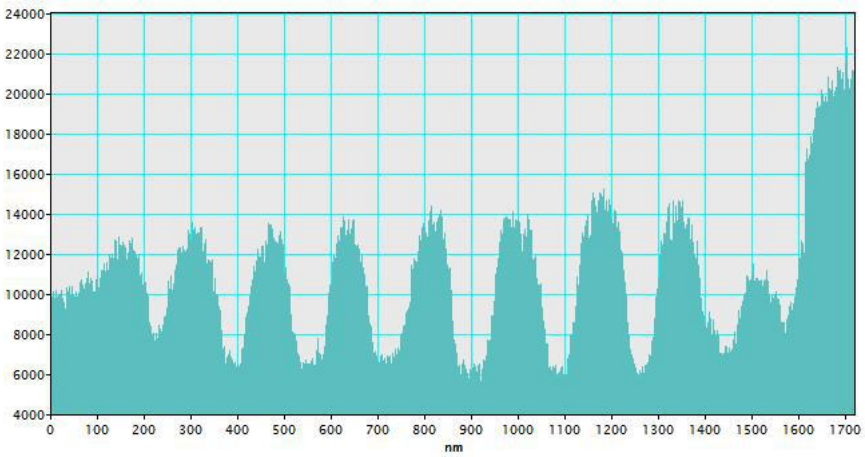

Figure 1.6: *Analysis of the multilayer structure in figure 1.5. Graph shows individual layer thickness (nm), each peak and trough indicate a single layer of chitin and air respectively.*

1.5 Materials and methods

1.5.1 Apparatus

To collect spectral data of elytra throughout this investigation an optical spectrometer and goniometer were used (figure 1.7).

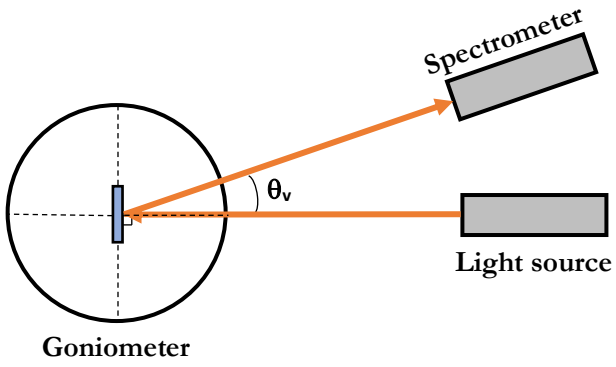

Figure 1.7: *Vertical perspective of equipment (orange arrows represent emitted and reflected light)*

Figure 1.7 shows the general setup for the collection of data used in chapters 1, 2 and 3 to measure reflected wavelengths and the corresponding relative intensities. The receiver arm (light source) is kept normal to the plate that supports the elytron piece for every angle of view (θ_v). The light source is an Ocean Optics [12] HL-2000 Tungsten Halogen bulb which is focused onto the surface of the elytron. The angle of view of the spectrometer is measured using the goniometer which also supports the elytron, with the smallest possible angle of view being 10° (when the light source is facing normal to the surface). The distances of both arms from the goniometer were kept constant for every experiment and for every individual viewing angle.

Furthermore, it is important to note that the term "angle of incidence" refers to the angle of incident light (used when describing equations), whereas "angle of view" refers to the angle of the receiver arm relative to the normal. Moreover, the mathematical equations are valid for either type of measurement and the angle of view was chosen because it ignores any reflective phenomena of light that would otherwise be present with a changing angle of incidence. This allows for easier modelling in chapters 2 and 3, however, a changing angle of incidence is dealt with in chapter 4.

1.5.2 Methods of data collection

SpectraSuite [12] was the software used to collect the spectral data. For every angle of view, a spectrum is recorded which can then easily be converted into raw data and analysed in an Excel spreadsheet. Before a spectrum could be recorded, it was necessary to collect a dark spectrum as it disregards any background light that may be received by the spectrometer. The dark spectrum was then removed before recording the spectrum of the elytron [12]. During the collection process it was important to ensure the plate and elytron were not tilted vertically or horizontally on the goniometer as this would change the values of reflected wavelengths and relative intensities for a given angle of view. Moreover, the boxcar width for every spectrum was kept at 5 units to ensure there were no changes to spectral dimensions.

1.6 Spectral analysis

When a spectrum is collected, SpectraSuite records reflected wavelengths between 350-1000nm in 1nm intervals, when ideally, we want to focus on the range of wavelengths of the broad band light source which covers the visible spectrum of (390-700nm). Referring back to sections 1.2 and 1.3, it was established that for every angle of incidence only certain wavelengths of white light will satisfy the condition of constructive interference. These wavelengths are the dominant reflected wavelengths (λ_{max}) and thus have a higher relative reflected intensity.

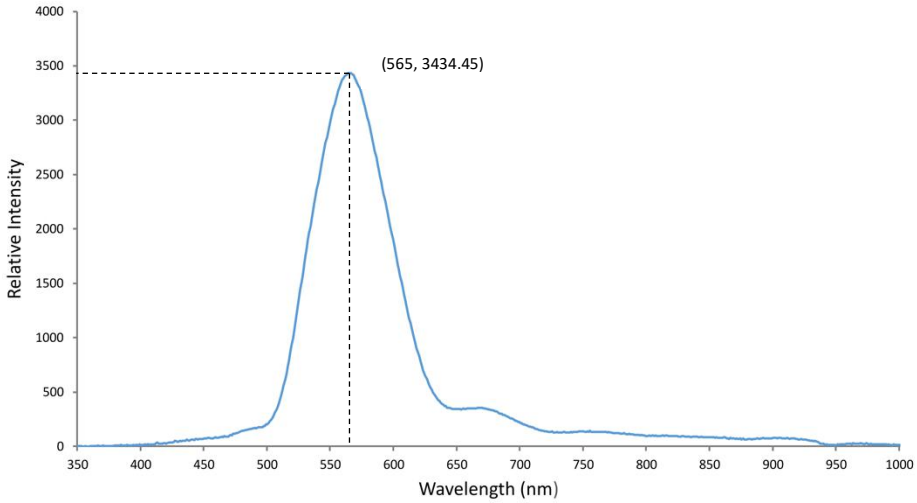

Figure 1.8: *Spectrum taken at 10° angle of view shows a dominant reflection peak at 565nm.*

In figure 1.8, a large reflection peak can be seen indicating that the dominant reflected wavelength is 565nm. Therefore, given the correct parameters it can be shown that a wavelength of 565nm satisfies the equation for constructive interference in a multilayer reflector when the angle of incidence is 10°. A wavelength of 565nm lies within the green region of the colour spectrum approximately 530-570nm as shown in figure 1.9. It was found that the *C. wallacei* elytra had consistent initial dominant reflection peaks that lay within this region, however multiple experiments showed large variability (figures 1.11-1.14).

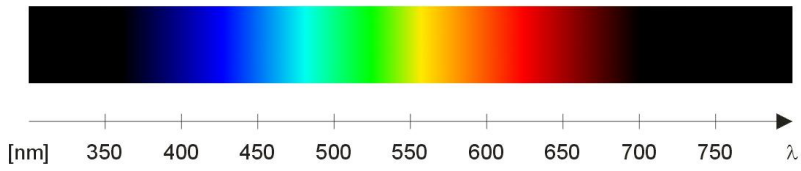

Figure 1.9: *The colour spectrum*

As the angle of view increases, the relative intensity of the reflection peak decreases (figure 1.10) meaning the reflected colours are reducing in brightness.

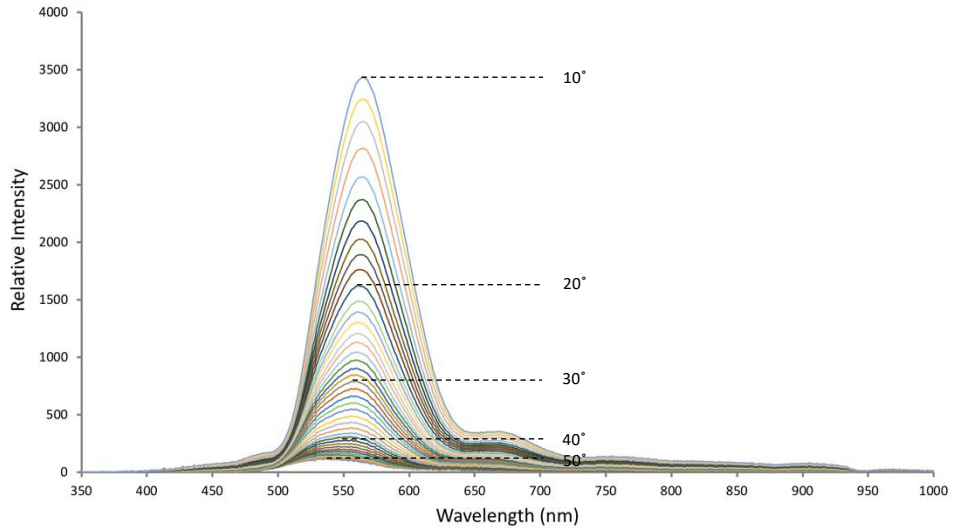

Figure 1.10: *Spectra taken from 10˚ to 50˚ in 1˚ intervals*

1.6.1 Blueshift of the λ_{max} peak

Through the further analysis of spectra, it was found that the dominant reflected wavelength reduced as the angle of view increased confirming that the *C. wallacei* elytra are indeed iridescent. The reduction in wavelength is also known as blueshift. Several experiments were done on different elytra and all showed similar blueshifts in wavelength up to 40˚, figures 1.11-1.14 demonstrate this for different initial values of λ_{max}. Figure 1.11 showed the largest blueshift, and figure 1.12 showed the smallest.

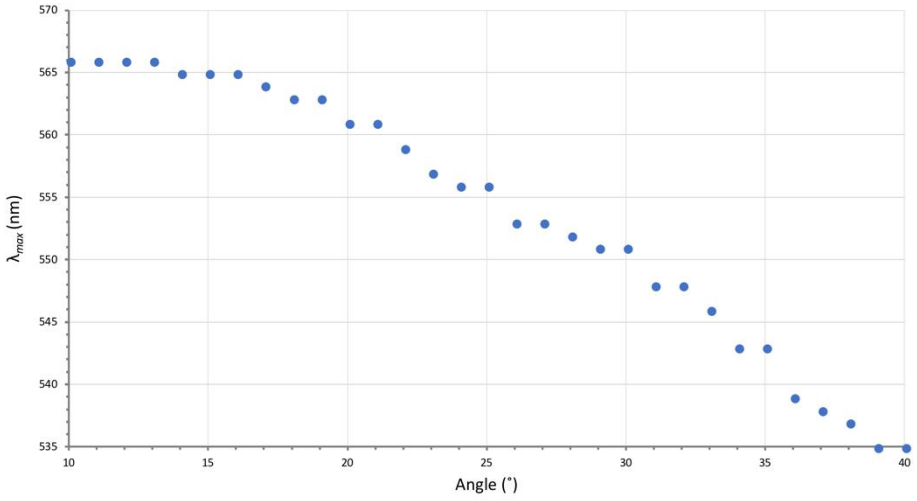

Figure 1.11: *Initial peak at 566nm decreases to a minimum of 535nm, $\delta\lambda$=31nm*

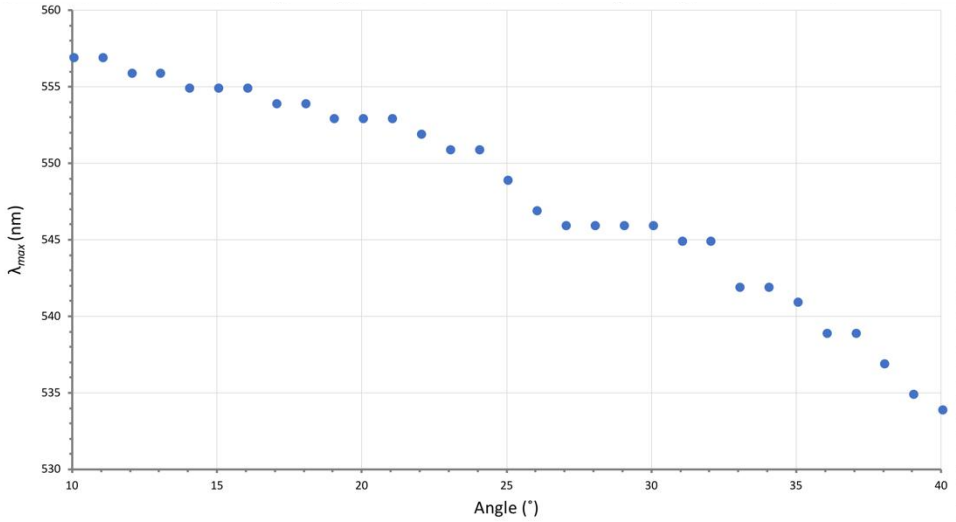

Figure 1.12: *Initial peak at 557nm decreases to a minimum of 534nm, $\delta\lambda$=23nm*

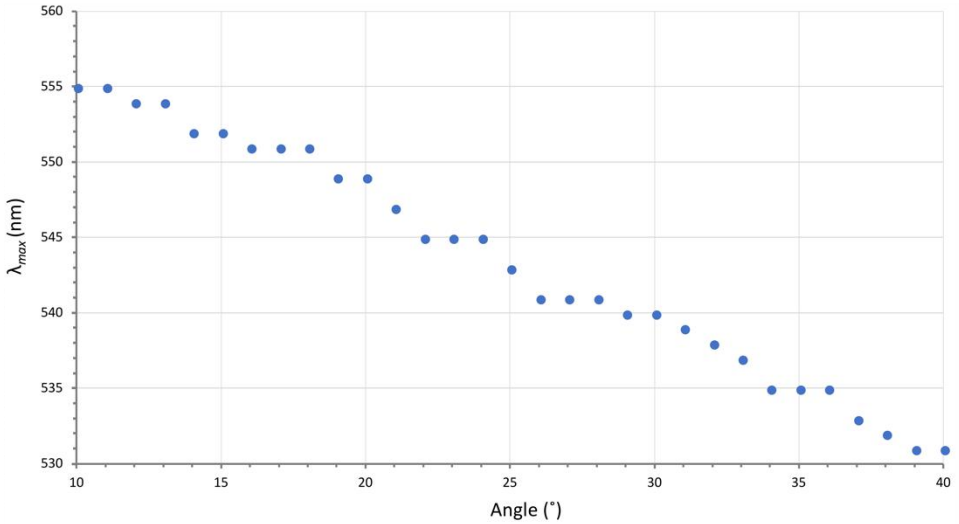

Figure 1.13: *Initial peak at 555nm decreases to a minimum of 531nm, $\delta\lambda$=24nm*

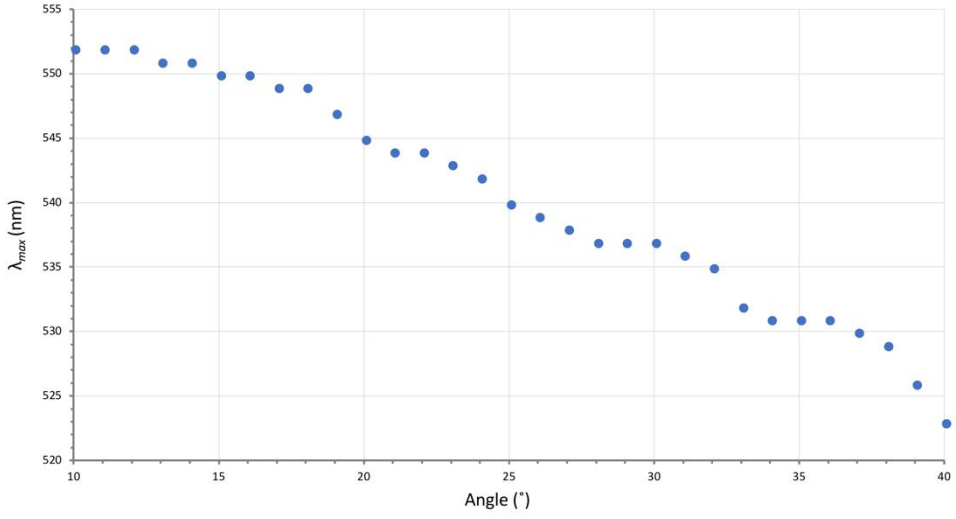

Figure 1.14: *Initial peak at 552nm decreases to a minimum of 523nm, $\delta\lambda$=29nm*

1.6.1.1 Pearson correlation coefficient

The Pearson correlation coefficient (PCC) is a measure of the linear correlation in bivariate data. It takes values between +1 and -1 where 1 is a total positive linear correlation, 0 is no linear correlation, and -1 is a total negative correlation. It is represented by the letter ρ (rho) which is calculated by the formula,

$$\rho_{X,Y} = \frac{\operatorname{cov}(X,Y)}{\sigma_X \sigma_Y},$$

where X and Y are variables, *cov* is the covariance and σ is the standard deviation.

This technique was used to measure the linear correlation between λ_{max} and the viewing angle in figures 1.11-1.14 as shown in the table below.

Figure number	PCC
1.11	-0.9805
1.12	-0.9790
1.13	-0.9955
1.14	-0.9908

Figure 1.15: Table showing PCC values

Figure 1.15 shows that the data in all figures have very high PCC values which implies that there is a very strong negative linear relationship between the viewing angle and λ_{max} up to 40°, with the average value being -0.9865.

1.6.1.2 Spectral richness

Spectral Richness (SR) is the rate of change of λ_{max} with respect to angle of incidence [13]. It is given by the equation,

$$SR = \lim_{\delta\theta \to 0} \frac{\delta\lambda_{\max}}{\delta\theta} = \frac{d\lambda_{\max}}{d\theta}.$$

Since we know the equation for constructive interference in a multilayer reflector (1), the formula for spectral richness can be calculated using basic differentiation techniques (m=1),

$$SR = -\left(\frac{2d_1 {n_0}^2 \sin\theta_0 \cos\theta_0}{\sqrt{{n_1}^2 - {n_0}^2 \sin^2\theta_0}} + \frac{2d_2 {n_0}^2 \sin\theta_0 \cos\theta_0}{\sqrt{{n_2}^2 - {n_0}^2 \sin^2\theta_0}} \right).$$

If we assume the relationship between λ_{max} and angle of view is perfectly linear, where the PCC is equal to 1, then we would expect the spectral richness to be constant for every viewing angle. Since all the data sets (figures 1.11-1.14) showed very high PCC values then it's suitable to implement a regression line which makes it possible to find the average value for the spectral richness by calculating the gradient of the regression line.

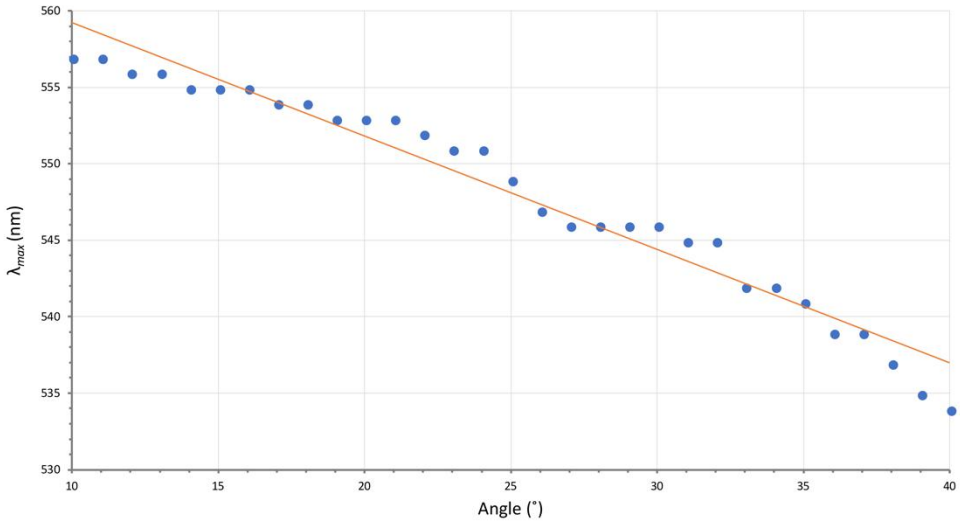

Figure 1.16: *Regression line (orange) applied to data in figure 1.12*

By incorporating this method for every data set, the average spectral richness can be calculated.

Figure number	Average SR (nm/°)
1.11	-1.12
1.12	-0.74
1.13	-0.84
1.14	-0.94

Figure 1.17: *Table showing average spectral richness found by the gradient of the regression line*

From figure 1.17 its clear to see that figure 1.11 has the largest spectral richness which follows from the fact that it showed the largest blueshift in wavelength ($\delta\lambda$=31nm).

1.7 Modelling changes in λ_{max}

Mathematically modelling changes of dominant reflected peaks requires a simplification of the physical system in order to apply previous mathematical equations. To do this we assume:

- The initial entrance medium is air (not including the multilayer structure).
- The multilayer structure is comprised of alternating parallel layers of chitin and air where each layer has the same width.
- The two media (chitin and air) are both isotropic[3] and homogeneous[4] with refractive indices of 1.56 [1] and 1 respectively.

[3] Isotropic: The properties of a material are invariant under rotational transformations in the material
[4] Homogenous: The properties of a material do not depend on spatial position

From section 1.3, the equation for constructive interference in a multilayer is given by (1):

$$m\lambda = 2\left(d_1\sqrt{n_1^{\,2} - n_0^{\,2}\sin^2\theta_0} + d_2\sqrt{n_2^{\,2} - n_0^{\,2}\sin^2\theta_0}\right).$$

For the system described above, the above equation can be rewritten as (m=1),

$$\lambda = 2d\left(\sqrt{n_1^{\,2} - k\sin^2\theta_0} + \sqrt{n_2^{\,2} - k\sin^2\theta_0}\right), \qquad (2)$$

where k is a constant and d is the thickness of a single layer. The new spectral richness can be found by differentiating equation (2) to give,

$$SR = -\left(\frac{2dk\sin\theta_0\cos\theta_0}{\sqrt{n_1^{\,2} - k\sin^2\theta_0}} + \frac{2dk\sin\theta_0\cos\theta_0}{\sqrt{n_2^{\,2} - k\sin^2\theta_0}}\right). \qquad (3)$$

1.7.2 The program

```
import numpy as np
import matplotlib.pyplot as plt

n1=1.56
n2=1
i=10
t=40

my_lists=["ag","wl","sr","difference"]
for j in my_lists:
    exec(j+'=[]')

k= (constant)
max_wavelength= (nm)
d=float(max_wavelength/(2*(np.sqrt((n1**2)-(k)*((np.sin(np.radians(10)))**2))+np.sqrt((n2**2)-(k)*((np.sin(np.radians(10)))**2)))))

while i<=t:
    max_lambda=2*(d*np.sqrt((n1**2)-(k*(np.sin(np.radians(i)))**2))
    +(d*np.sqrt((n2**2)-(k*(np.sin(np.radians(i)))**2))))
    wl.append(max_lambda)

    spectral_richness=-((2*d*k*(np.sin(np.radians(i)))*(np.cos(np.radians(i)))/(np.sqrt((n1**2)-(k*(np.sin(np.radians(i)))**2))))
    +(2*d*k*(np.sin(np.radians(i)))*(np.cos(np.radians(i)))/(np.sqrt((n2**2)-(k*(np.sin(np.radians(i)))**2)))))/(180/np.pi)
    sr.append(spectral_richness)
    ag.append(i)
    i+=1

for i in wl:
    t=round(max(wl)-i,3)
    difference.append(t)
f=open('wl_difference.txt','w')
for i in difference:
    f.write("%s\n"%i)
f.close()
```

(2)

(3)

Figure 1.18: *The main section of the code responsible for the calculations of λ_{max} and SR for different angles of incidence.*

1.7.2.1 Layer thickness "d"

The data obtained from the TEM images showed the layer thicknesses in the multilayer were on average 100nm. However, the distances were shown to vary from 80-100nm. This range produced an even larger spread for the calculated values of λ_{max} using equation (1). Furthermore, spectral data obtained in section 1.6.1 (figures 1.11-1.14) also showed large variability in the initial value for the dominant reflected wavelength at 10°. Therefore, I concluded that a program which calculated the layer thickness when given an initial value for λ_{max} was more suited in modelling the data. The calculated layer thicknesses could then be compared with the average recorded value of 100nm obtained from TEM images.

1.7.2.2 Constant "k"

Before the constant *k* was implemented, it was evident that the data in figures 1.11-1.14 did not follow the predictions calculated by equation (1). An example of this can be shown in figure 1.19, where the blue curve is the model, and the red dots are the data points.

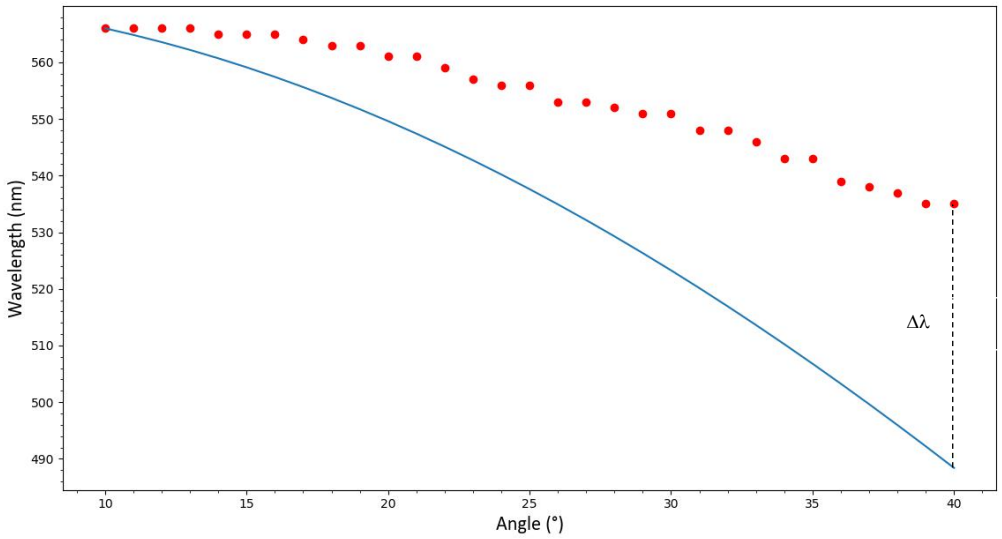

***Figure 1.19**: Model applied to data from figure 1.11. When k=1, Δλ=46.6nm*

As the value of *k* changes, the dominant reflected peak calculated at 40° also changes while keeping the initial value at 10° the same. Through trial and error, the constant *k* can be found when the calculated value of λ_{max} matches that of the data at 40°. The constant was therefore implemented to produce equation (2). The purpose of this was to investigate how well data matched the predicted values of the equation in the same wavelength range, $\delta\lambda$, ($\Delta\lambda$=0).

1.7.3 Data analysis

The model was applied to data in figures 1.11-1.14 from section 1.6.1. The results are shown below in figures 1.20-1.23.

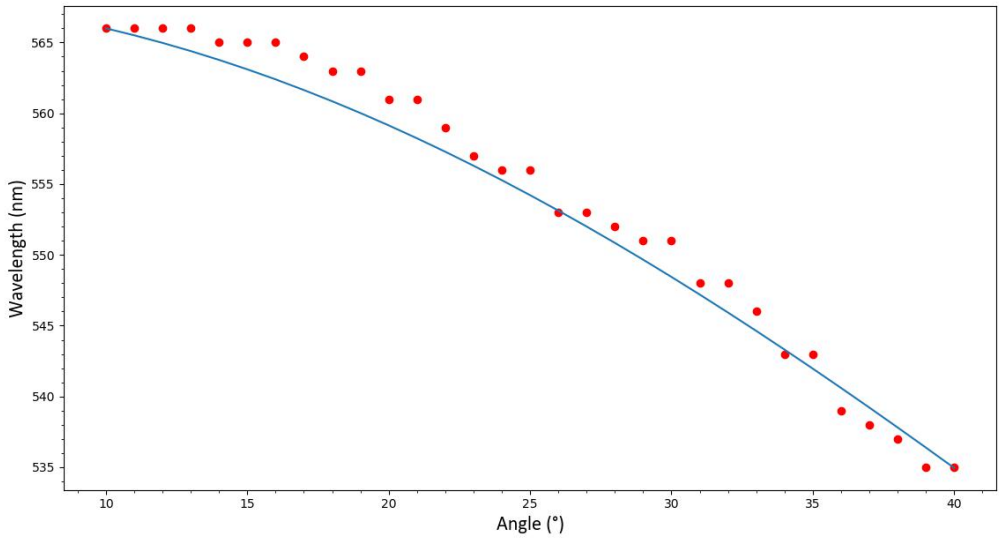

Figure 1.20: *Model applied to figure 1.11, k=0.428*

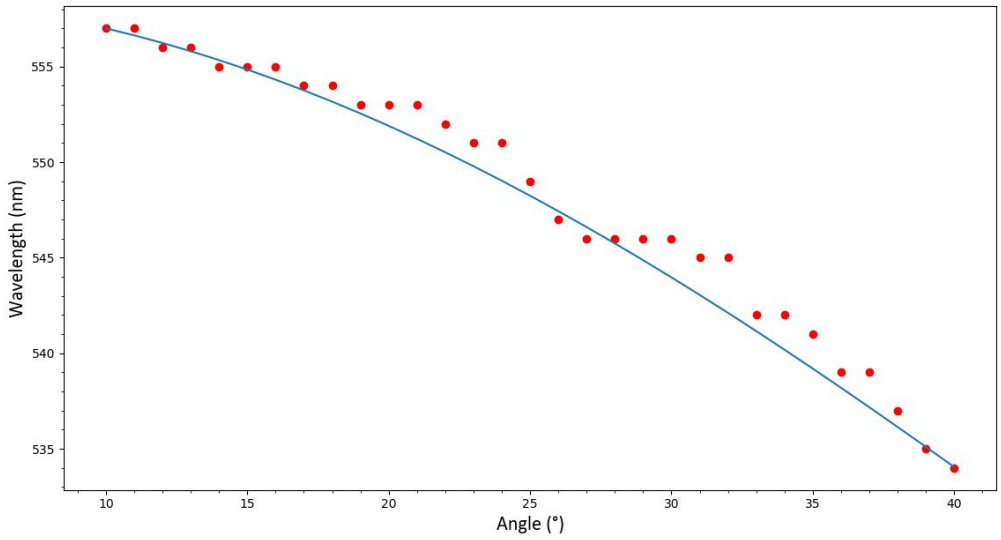

Figure 1.21: *Model applied to figure 1.12, k=0.325*

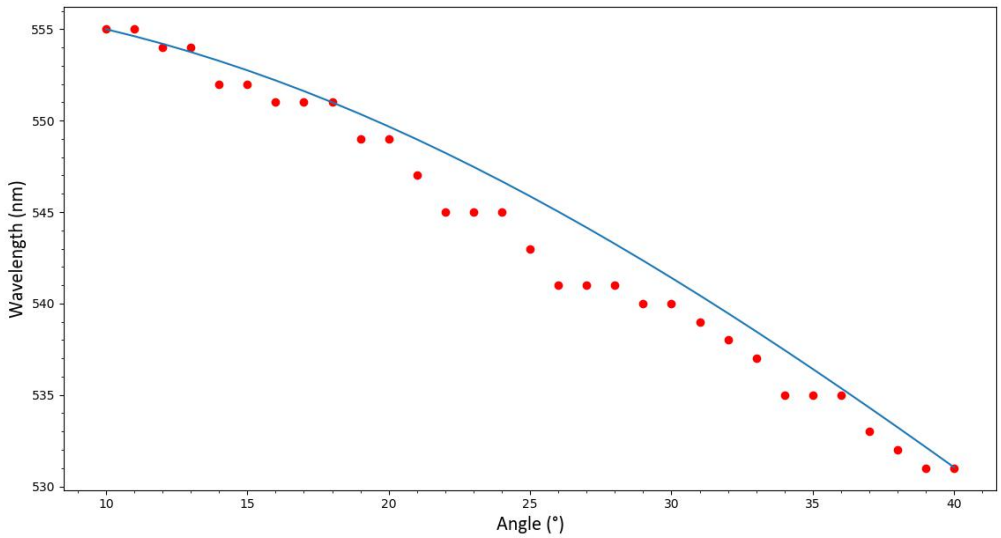

Figure 1.22: *Model applied to figure 1.13, k=0.34*

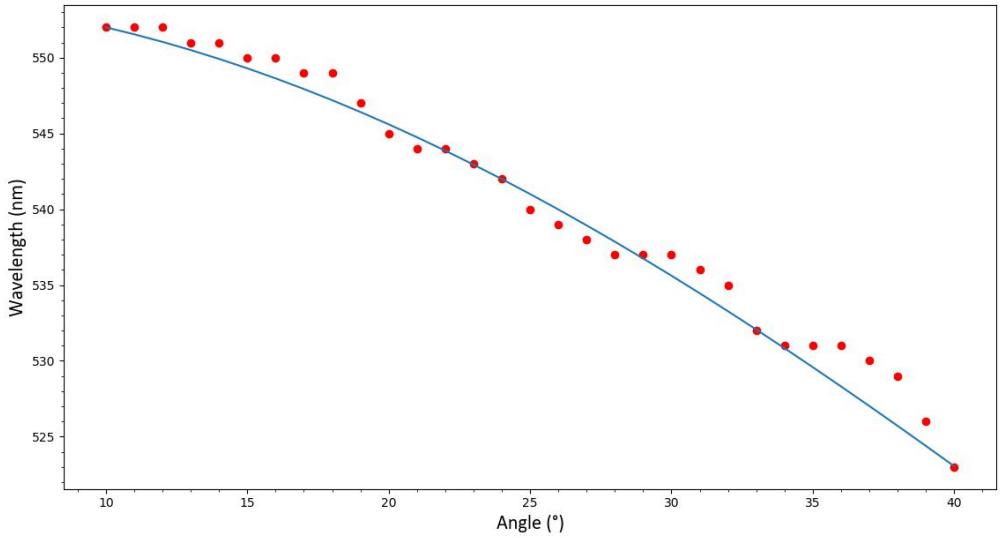

Figure 1.23: *Model applied to figure 1.14, k=0.41*

The graphs show that the predicted values for λ_{max} do not follow a linear relationship as the data implied previously. This of course makes sense as equation (2) is a linear combination of cosine functions.

1.7.3.1 Root-mean-square deviation

The root-mean-square deviation (RMSD) is a measure of the differences between values predicted by a model and the values actually observed. The RMSD represents the sample standard deviation of the differences between predicted and observed values. It is calculated by the formula,

$$RMSD = \sqrt{\frac{1}{T}\sum_{t=1}^{T}(\widehat{y}_t - y_t)^2},$$

where $\widehat{y}_t$ are the predicted values, y_t are the observed values and T is the total number of observed values. This method was used to measure how well the model predicts the data above.

Figure number	RMSD (nm)	NRMSD (%)
1.20	1.59	5.13
1.21	1.20	5.20
1.22	1.76	7.33
1.23	1.31	4.52

Figure 1.24*: Table showing RMSD and NRMSD for the 4 data sets.*

The calculations for RMSD for figures 1.20-1.23 turned out to be very small. The normalized root-mean-square deviation (NRMSD) is the RMSD as a percentage of the total blueshift $\delta\lambda$. Values as low as these imply the model is very good at predicting the observed data values and can therefore be considered an accurate model.

1.7.3.2 Spectral richness

From equation (3) it is clear to see that spectral richness is not constant for every angle of view (figure 1.25) which contradicts the very high PCC values calculated in section 1.6.1.1.

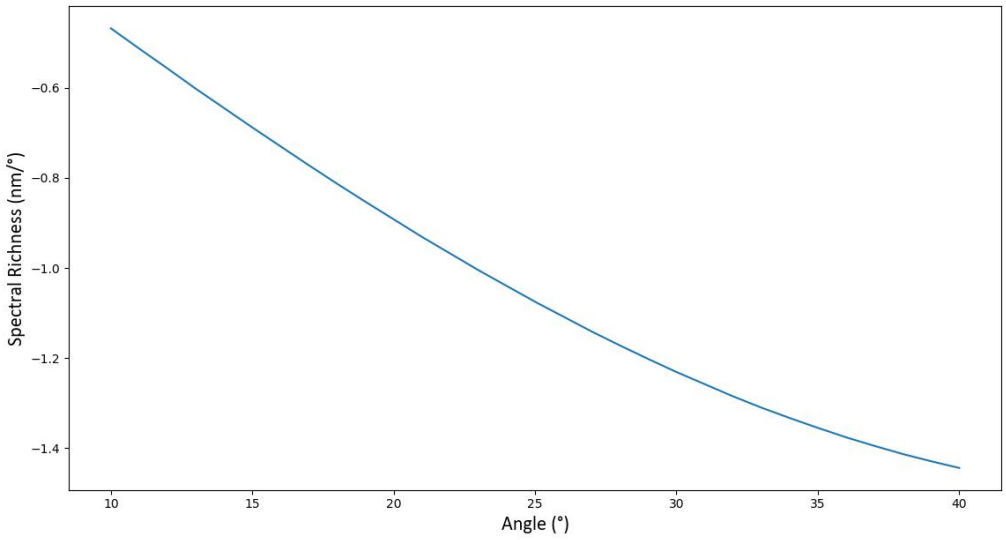

Figure 1.25: *Spectral Richness calculated for modelled data in figure 1.20*

The accuracy of the model can be tested further by comparing the average spectral richness for experimental data (figure 1.17) and modelled data.

Figure number	Average SR *(model)* (nm/˚)	Average SR *(data)* (nm/˚)	ΔASR (nm/˚)
1.20	-1.03	-1.12	0.09
1.21	-0.76	-0.74	0.02
1.22	-0.80	-0.84	0.04
1.23	-0.96	-0.94	0.02

Figure 1.26: *Table showing average spectral richness for modelled and observed data up to 40˚, where ΔASR is the difference between modelled and observed values.*

Figure 1.26 shows the average spectral richness of modelled and observed data are very close with the average difference being 0.0425 nm/˚. This result agrees with the RMSD's in that the model predicts the data very well.

1.7.3.3 Calculated values for "d"

Figure number	Layer thickness (nm)
1.20	111
1.21	110
1.22	109
1.23	110

Figure 1.27: *Table showing calculated layer thicknesses for each model*

From figure 1.27, the average predicted layer thickness is 110nm. When compared to the actual average layer thicknesses from multilayer images (100nm), the difference is 10nm.

1.8 Water treatment

The purpose of the investigation was to see how changing the refractive index of some of the layers in the multilayer structure would have an effect on the dominant reflected wavelength and iridescence as a whole. Water treatment is the process of soaking an elytron in water at room temperature for 2-3 weeks in order to observe a colour change from the normal green hue to darker yellow colours. Spectra of the elytron were taken before and after the treatment to allow for spectral and mathematical comparisons. Before taking spectra of the treated elytron, any excess water was removed from its surface to ensure the only water present was within the elytron.

In section 1.4 we established that the multilayer structure in the *C. wallacei* elytron is made up of alternating layers of chitin and predominantly air. The purpose of water treatment was to allow water molecules to move through pores in the multilayer structure and to ultimately replace the air layers with water. This would produce a multilayer stack consisting of mainly chitin and water. The treatment would stop when no apparent colour changes were taking place which would suggest the diffusion of water molecules through the pores had ceased. Furthermore, water treatment was chosen due to the individual water molecules being very small compared to other liquids. Small molecular diameters ensured the molecules had a greater probability of diffusing through the pores on the surface of the elytron. An image of a water treated elytron can be found on page 52.

1.8.1 Spectral analysis

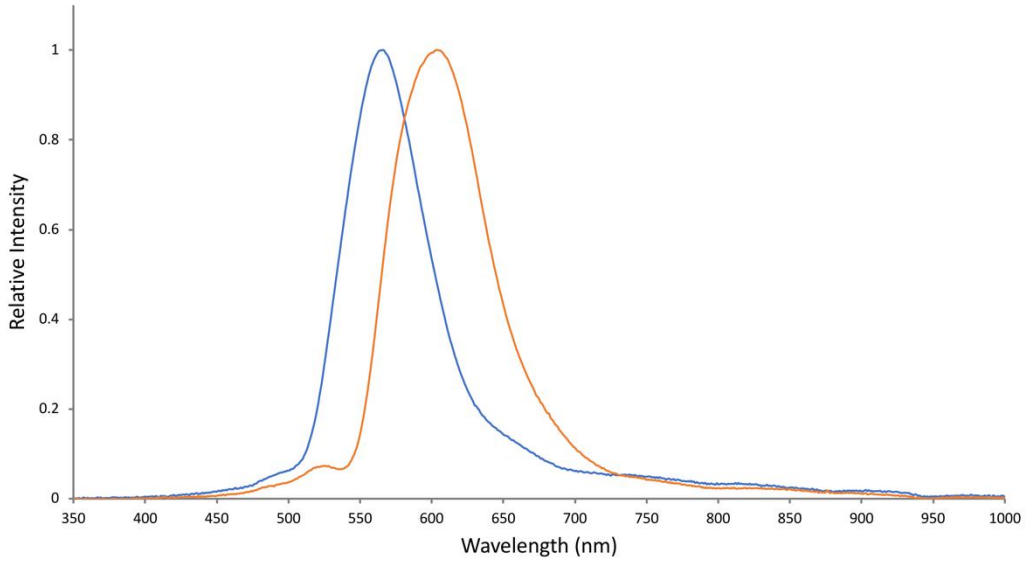

Figure 1.28: *Two spectra taken at an initial angle of 10˚ of an elytron before treatment (blue) and after treatment (orange), λ_{max} of blue spectrum is 566nm and 604nm for the orange spectrum*

Figure 1.28 shows that water treatment caused the λ_{max} peak to shift to the right towards longer wavelengths (redshift) relative to the spectra taken of the same elytron, at the same angle of view before treatment. This produced a total initial shift of $\Delta\lambda_{max}$ =38nm. It is also worth noticing the

shape of the orange spectrum, since it is clear to see a second peak has become more prominent at around 525nm possibly due to the absorption of wavelengths of light around 540nm.

Spectra taken before treatment showed a total blueshift of the maximum peak of 23nm, while the spectra recorded from the treated elytron showed a considerably larger shift of 37nm (figure 1.30). Therefore, the change in wavelength for the treated elytron is 14nm larger.

1.8.2 The model

When modelling data for treated elytra, the second medium is supposedly water which has a refractive index of 1.33. When implemented in the program (figure 1.18) for an arbitrary layer thickness, the initial value of λ_{max} also increases which agrees with the spectra shown in figure 1.28.

In addition, the model calculated (under no influence of data, k=1) the blueshift before treatment to be 78nm and after treatment to be 60nm (figure 1.29). However, this contradicts the observed values in which the treated elytron had the greatest blueshift. The model predicts the blueshift for the non-treated elytron to be 18nm larger.

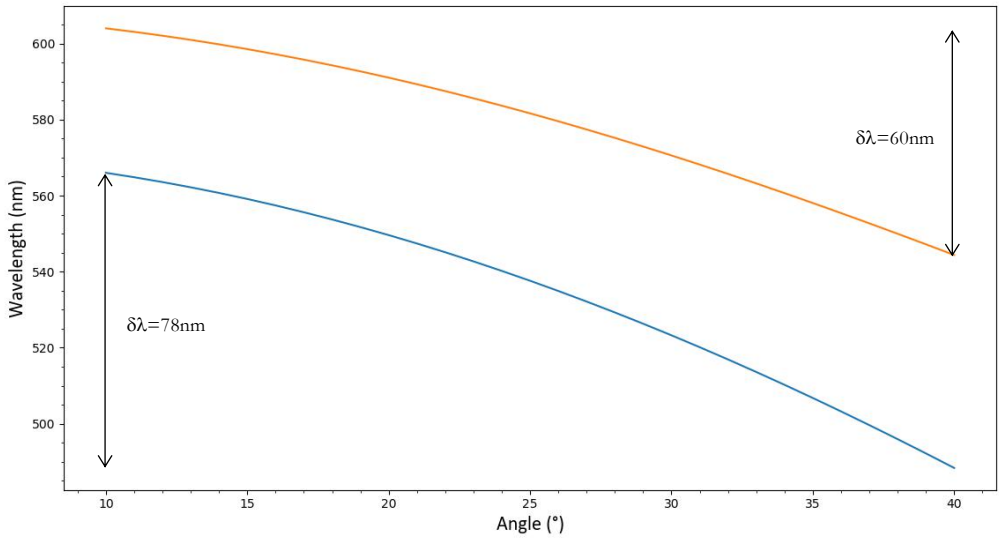

Figure 1.29: *Graph showing predicted values for λ_{max} before (blue) and after treatment (orange), k=1.*

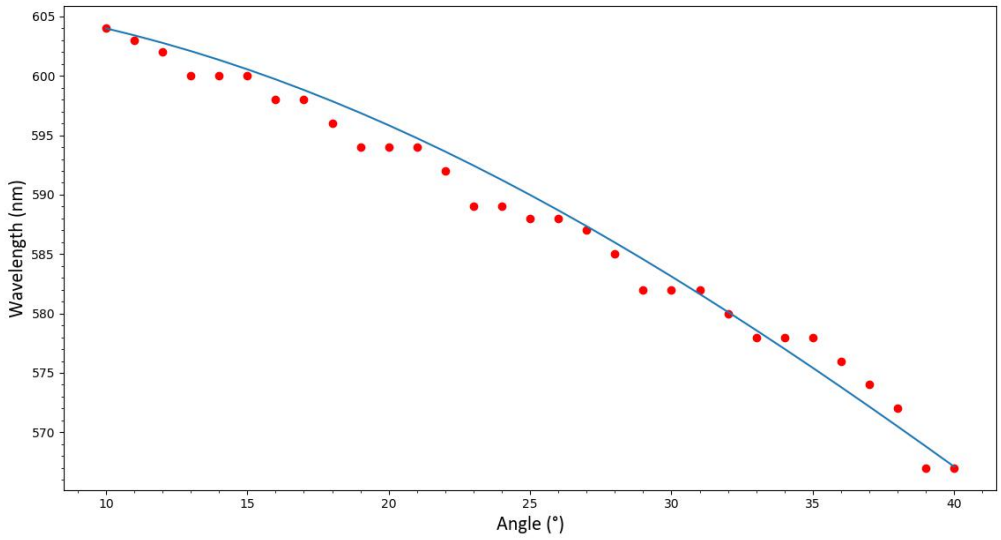

Figure 1.30: *Model applied to data (water treated elytron), k=0.635*

The RMSD for figure 1.30 was calculated to be 1.62nm and the NRMSD was 4.38%. Both these values imply the model is still very accurate, and able to predict the trends in data effectively.

1.8.2.1 Calculated values for "d"

From the model in figure 1.30, the layer thickness was calculated to be 105nm which is 5nm smaller than the average values for *d* predicted for non-treated elytra. Moreover, it more closely matches the observed value of 100nm which implies there could be some uncertainty in the medium for the second layer in the multilayer structure which is considered to be mostly air.

Chapter 2: Modelling Relative Intensities

Throughout the previous investigations, it was noticed through spectral analysis that the relative intensities of the dominant reflected wavelength peaks would decrease with increasing angle of view as shown in figure 1.10. Therefore, it was necessary to set up an original model that tries to predict the changes in intensity which would then be applied to the model for spectral curvature in the next chapter. Furthermore, it is important to note that the mathematical ideas and corresponding code in this chapter are completely my own and will contain broad approximations based on mathematical theory, the limitations to which are covered in the conclusion.

2.1 Radiometric definitions

The term "intensity" is rather ambiguous and can have various mathematical definitions depending on what is being measured. The radiometric terms and definitions below are of main interest to the context of the modelling:

- *Radiant Intensity:* The radiant flux emitted, reflected, transmitted or received, per unit solid angle [14] given by the partial derivative,

$$I_{e,\Omega} = \frac{\partial \Phi_e}{\partial \Omega},$$

  where, Φ_e is the radiant flux and Ω is the solid angle[5]. Radiant flux is simply the radiant energy emitted, reflected, transmitted or received per unit time.

- *Radiance :* The radiant flux emitted, reflected, transmitted or received by a given surface, per unit solid angle per unit projected area [15] given by the equation,

$$L_{e,\Omega} = \frac{\partial^2 \Phi_e}{\partial \Omega \partial A \cos\theta},$$

  where, $A\cos\theta$ is the projected area[6]. Radiance is important in this context as it specifies how much power reflected by the elytron surface will be received by the spectrometer directed at

[5] A two-dimensional angle subtended by any part of a spherical surface of unit radius at its centre
[6] The area of the surface projected normally to the direction of view

the surface from a given angle of view. In radiometry, radiance is sometimes loosely referred to as the perceived "brightness" of a surface.

2.2 Inverse square law

The inverse square law states: *"The intensity of light emitted from a point source, which radiates equally in all directions, is inversely proportional to the square of the distance from the light source. [16]"*

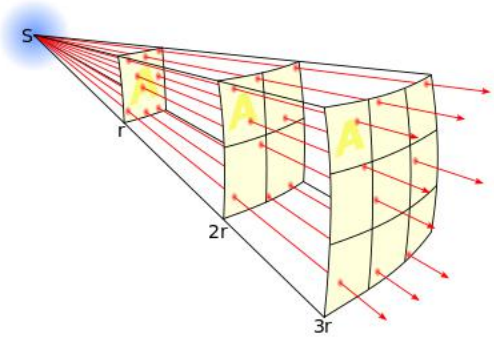

Figure 2.1: *Demonstration of the inverse square law [16]*

As shown in figure 2.1, as the distance from the source increases, *r,* the area, *A*, increases in proportion to the distance. The area represents the area of a sphere with the radius being the distance from the source. The red lines represent the flux emanating from the source, and it can be seen that the density of the flux lines decrease as *r* increases. The law can be stated as an equation,

$$I \propto \frac{1}{r^2}.$$

2.3 Reflection

Specular reflection is a term to describe reflection off a smooth surface, such as a mirror, in which each incident ray is reflected at the same angle to the surface normal as the incident ray [17]. In other words, the light is reflected into a single-outgoing direction. This is also known as *the law of reflection* as shown in figure 2.2.

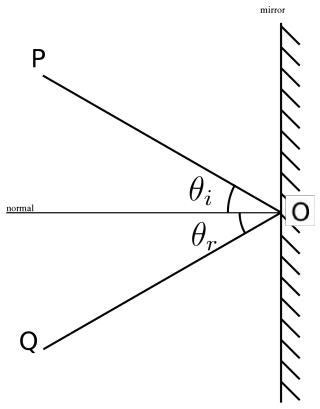

Figure 2.2: *Demonstration of the law of reflection, where P and Q represent the incident and reflected light respectively and* $\theta_i = \theta_r$

Diffuse reflection is the opposite of specular reflection in which light incident upon a rough surface is scattered at various angles.

2.4 The model

2.4.1 Projected viewing areas

As established in the apparatus section (1.5.1), light is incident along the normal of the elytron surface with the observer (receiver arm) rotating about the point at which the normal line intersects the flat plate supporting the elytron piece (figure 2.3). In addition, when the light source is kept at a 10cm separation from the plate, the light beam produces a perfect circle of incident light on a flat surface with a diameter of 0.5cm.

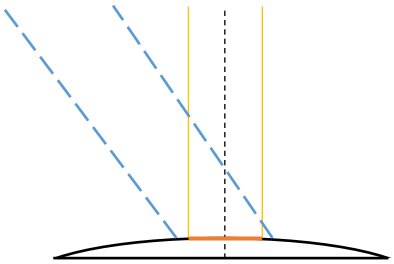

Figure 2.3: *Cross section showing incident beam of light at normal incidence (yellow) with diameter of 0.5cm (orange), and the field of view of the entrance pupil (blue) on the receiver arm.*

At a normal angle of view, the area of the surface covered by the entrance pupil is also a circle with diameter of 0.5cm. In addition, it was shown through varying the angle of incidence that the area of light projected onto the surface would increase as the angle of incidence increased. Therefore, the same principle must hold true for the viewing area projected onto the surface as the angle of view increases (figure 2.4).

Figure 2.4: *Diagram showing vertical perspective of figure 2.3. Demonstration of increasing projected viewing area (blue) as the angle of view increases for constant angle of incidence (yellow). Angle of view increases from 0 ° left to right.*

From figure 2.4 it is clear to see that larger angles of view produce elliptical projected viewing areas where the minor diameter of any ellipse is the same as the incident light (0.5cm). Furthermore, this will only be the case if the surface of elytron in the *y* direction is perfectly flat. It is important to note the term "projected area" in the context of the model is different to the projected area in the equation for radiance. I came up with term to describe the area of the

elytron surface covered by the observing apparatus, which is the entrance pupil on the receiving arm.

2.4.2 Mathematical description for intensity

My model for relative reflected intensities was based off the relationship between angle of view and projected viewing area. The equation for radiance in section 2.1 involves an area term A, which is the area of the surface reflecting incident light. However, I have rewritten the projected area in the radiance equation $A\cos\theta$ in terms of the projected viewing area which depends on the angle of view and also the surface dimensions. Therefore, by assuming the solid angle and radiant intensity are constants I produced my own equation relating relative intensity and projected viewing area,

$$I = \frac{1}{A(\theta_v)}, \qquad (4)$$

Where I is the relative intensity or "brightness" of diffusely reflected light off the surface of the elytron and A is the projected viewing area which is a function of viewing angle. This equation follows a similar structure to the equation for the inverse square law.

When developing this model, various parameters were ignored or simplified:

- Cross-sectional surface of the elytron can be approximated by a function
- Surface of any elytron is perfectly smooth with similar surface dimensions
- A normal at any point along the normal line (figure 2.3) in the y direction should be perpendicular to y axis. (Elytron surface is flat in the y direction)
- Direction of specular reflection is parallel to the direction of incident light
- The projected viewing area at a given angle of incidence is independent of the distance between the elytron surface and receiver (solid angle is negligible)
- Relative intensity of reflected light beyond 60° is considered to be zero. This was concluded after multiple experiments on different elytra showed the angle of view at which the relative intensity was negligible was 60°

2.4.3 The program

A program was built to implement equation (4) to calculate the projected viewing areas and intensities at different viewing angles given accurate geometric parameters as established from experiments. The python package sympy was most useful for algebraic calculations and representing the physical system in terms of a single geometric system.

2.4.3.1 Rotating observer

From figure 2.3 it can be seen that the elliptical projected viewing areas are defined between two points on the elytron surface where the boundary lines of the observation pupil intersect the surface. Thus, the distance along the surface between these two intersection points will be the major diameter of the ellipse. The method to finding these intersection points was to first model the rotation of the observer about the origin and to find the equation of both boundary lines at a given angle of view (figure 2.5). Each boundary line has a distance of 0.25cm from the normal since the diameter of the projected viewing area is 0.5cm at 0°.

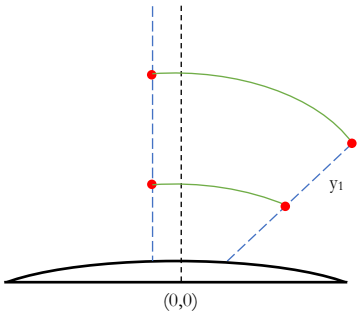

Figure 2.5: *Diagrams showing the rotation of two random points lying on one of the boundary lines to produce a new boundary line (y_1) which has been rotated about the origin.*

By assigning two random points on the initial boundary line at a theoretical angle of 0° and rotating them both about the origin by the same angle allowed the equation of the new rotated boundary line to be calculated. This was achieved by using a rotation matrix to rotate each point clockwise about the origin by a give angle. The matrix is given by,

$$\begin{pmatrix} \cos\theta & \sin\theta \\ -\sin\theta & \cos\theta \end{pmatrix}.$$

2.4.3.2 Intersection points and arc length

The cross section of the elytron surface was modelled as a cosine function implying perfect symmetry about the normal line. The equation for the cross section is given by,

$$y = h\cos\left(\frac{\pi x}{w}\right),$$

where, h is the maximum height of the elytron surface and w is the width of the cross section (figure 2.6).

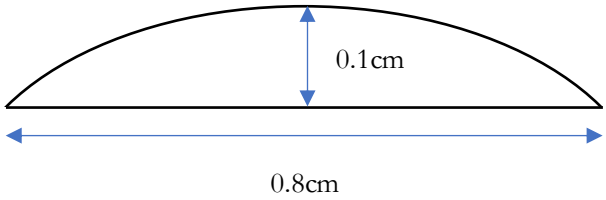

Figure 2.6: *Approximated dimensions of a typical elytron piece*

To find the intersection points of the boundary lines and the surface, the equation of the boundary line is set equal to the cosine function describing the cross-sectional surface and a value of x can be found. Once the two intersection points are known, the distance along the surface between the two intersection points can be calculated (figure 2.7). This is also known as the *arc length* and is computed by the integral,

$$L = \int_a^b \sqrt{1 + \left(\frac{dy}{dx}\right)^2}\, dx,$$

where *a* and *b* are the x-coordinates of the points of intersection and *y* is the equation of the cross section. However, when the integrand is simplified by finding the derivative, the integral above becomes an "elliptic integral of the third kind" [18]. This type of integral cannot be solved using normal integration methods, therefore I used a numerical method known as the *trapezium rule* to approximate the value of *L*.

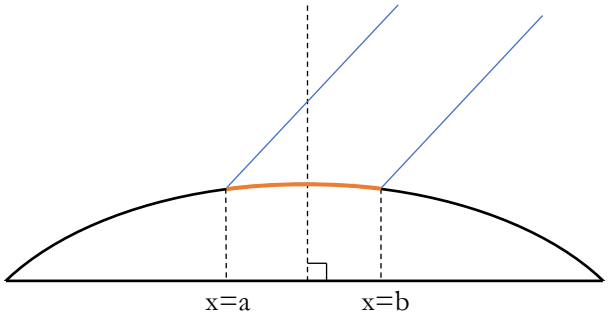

Figure 2.7: *Diagram of the intersection points and the corresponding arc length between them (orange)*

When the arc length has been computed, the area of the ellipse can be calculated by multiplying pi by the major and minor radii, in this case the major radii is half the arc length and the minor radii is 0.25cm. Thus, the projected area of view has been calculated. The relative intensity was then calculated by normalizing and taking the reciprocal of the areas (equation 4).

2.4.3.3 The program

```
import numpy as np
import sympy
import pylab
import scipy
from scipy import *
from sympy.solvers import nsolve
from sympy import *
import matplotlib.pyplot as plt
h=0.1
w=0.8
d=0.5
i=10
t=60

ln2_p1=[-d/2,1]
ln2_p2=[-d/2,2]
ln3_p1=[d/2,-1]
ln3_p2=[d/2,-2]
```

Rotation matrix

```
def transformation(point, angle, list1):
    a=[np.cos(np.radians(angle)), np.sin(np.radians(angle))]
    b=[-np.sin(np.radians(angle)), np.cos(np.radians(angle))]
    matrix=[a,b]
    point2=list(np.dot(matrix,point))
    list1.append(point2)

while i<=t:
    transformation(ln2_p1,i,ln2_p1_t)
    transformation(ln2_p2,i,ln2_p2_t)
    transformation(ln3_p1,i,ln3_p1_t)
    transformation(ln3_p2,i,ln3_p2_t)
    i+=1
    angle3.append(i)

while l<=len(ln2_p1_t)-1:
    ln2_p12_t.append([ln2_p1_t[l],ln2_p2_t[l]])
    ln3_p12_t.append([ln3_p1_t[l],ln3_p2_t[l]])
    l+=1
```

Equation of rotated lines

```
for i in ln2_p12_t:
    m=(i[1][1]-i[0][1])/(i[1][0]-i[0][0])
    l=(m*-i[0][0])+i[0][1]
    y=str(m)+"*x"+"+"+str(l)
    equations2.append(y)
for i in ln3_p12_t:
    m=(i[1][1]-i[0][1])/(i[1][0]-i[0][0])
    l=(m*-i[0][0])+i[0][1]
    y=str(m)+"*x"+str(l)
    equations3.append(y)
```

Points of intersection

```
for i in equations2:
    x=sympy.symbols('x')
    inter=nsolve(h*cos(pi*x/w)-eval(i),0)
    intersection2.append(inter)
for i in equations3:
    x=sympy.symbols('x')
    inter=nsolve(h*cos(pi*x/w)-eval(i),0)
    intersection3.append(inter)

for i in intersection2:
    if i>=-w/2:
        int2.append(i)
for i in intersection3:
    if i<=w/2:
        int3.append(i)

while p<len(int2):
    boundaries.append([int2[p],int3[p]])
    p+=1
```

Trapezium rule

```
def trapezium_rule(a, b, n):
    h=(b-a)/n
    s=np.sqrt(float(1+(-(h*np.pi/w)*np.sin(float(np.pi*a/w)))**2))
    +np.sqrt(float(1+(-(h*np.pi/w)*np.sin(float(np.pi*b/w)))**2))
    for i in range(1, n):
        s+=2*np.sqrt(float(1+(-(h*np.pi/w)*np.sin(float(np.pi*(a+i*h)/w)))**2))
    return (s*h/2)
```

Figure 2.8: *Main sections of the program responsible for calculating projected areas of view*

2.5 Fitting the model with data

For recorded spectra, it was ensured the incident beam of light covered a surface with similar if not exact dimensions used in the program where h=0.1 and w=0.8. The figures below show observed relative intensities (red dots) and the predictions from the model (blue lines) up to 40° angle of view.

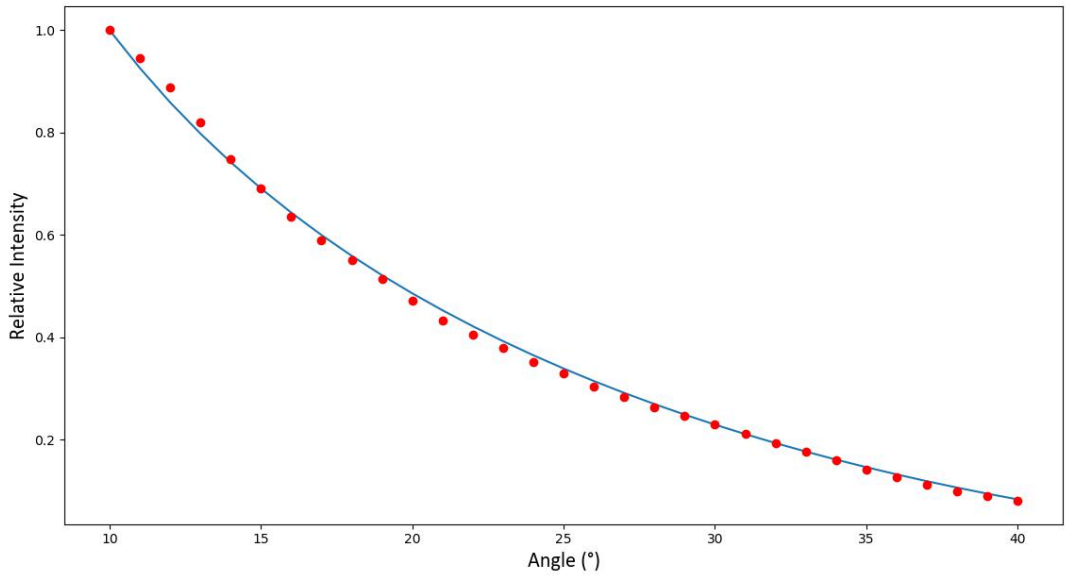

Figure 2.9

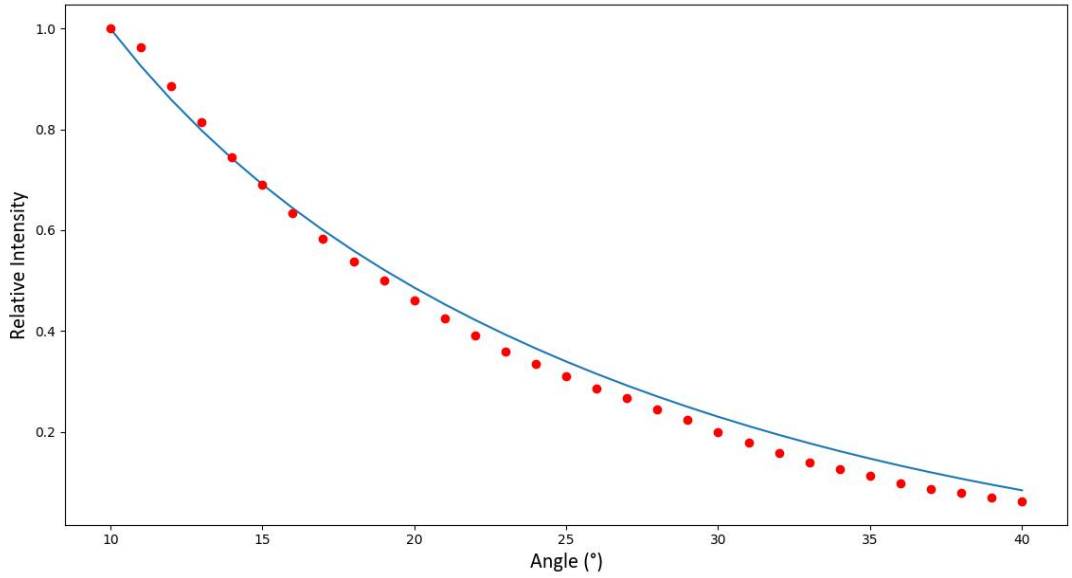

Figure 2.10

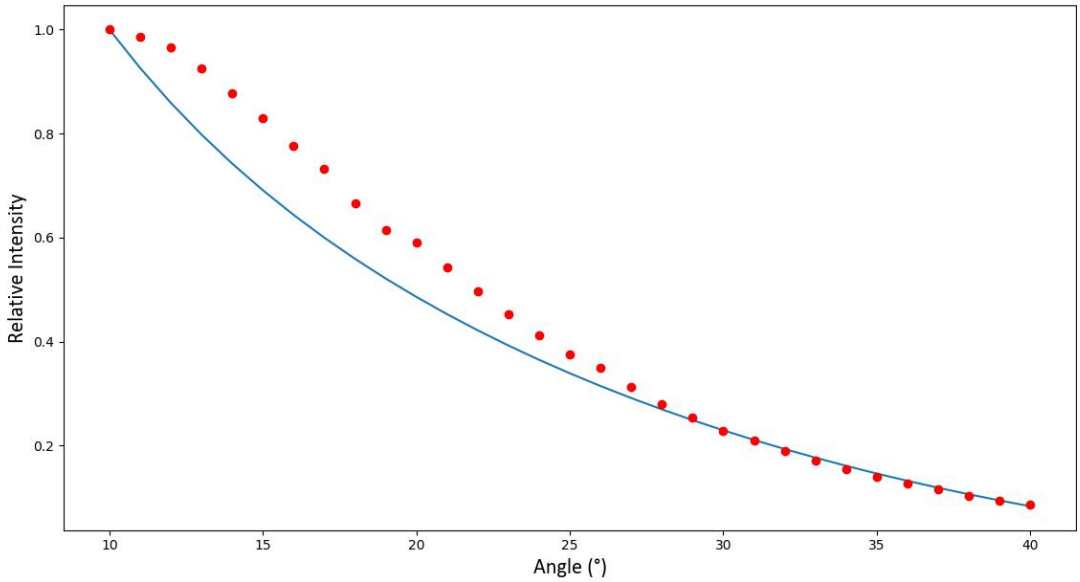

Figure 2.11

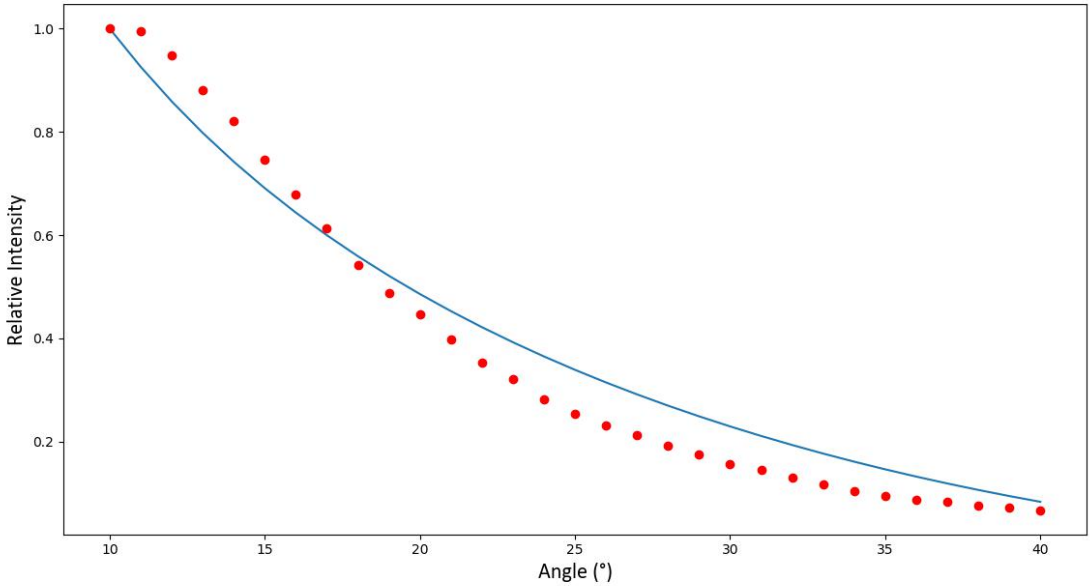

Figure 2.12

From a sample of 20 individual experiments, figures 2.9-2.12 represent the closest and the most extreme relationships between the model and the data.

Figure number	RMSD
2.9	0.01
2.10	0.03
2.11	0.07
2.12	0.06

Figure 2.13: *Table showing RMSD values*

From figure 2.13, the RMSD values are very small with the average being 0.04. Therefore, it can be established that the model predicts the data very well. It is worth noticing an initial increase in gradient can be seen in figures 2.11 and 2.22 between 10° and 15° which is characteristic of curved surfaces which can be accounted for in complex reflection models [19]. In addition, by changing the value of *h* in the model (the height of the cosine function) it was shown that an increasing value of *h* results in a faster initial decrease in relative intensity (figure 2.14).

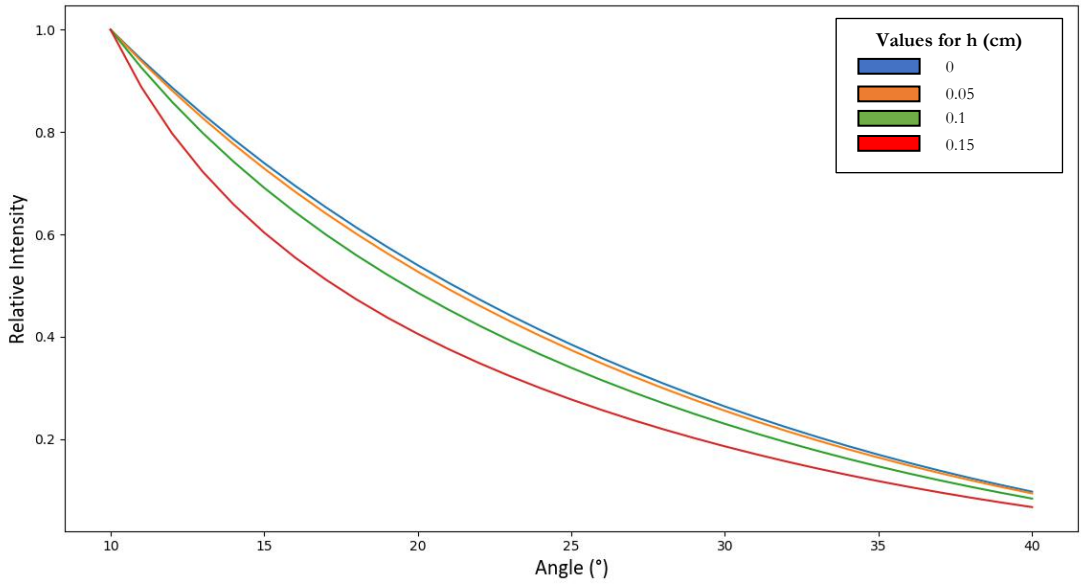

Figure 2.14

Chapter 3: Modelling Spectral Curvature

Modelling spectral curvature involves mathematically producing a spectrum which closely matches the observed spectrum from experimental data as seen in figure 1.8. Moreover, by using the models in previous chapters which describe how wavelength and relative intensity changes with viewing angle, it is possible to predict the spectral dimensions for a spectrum at any given viewing angle (figure 1.10).

3.1 Lagrange interpolation

Langrage interpolation is a mathematical technique which allows the trend in bivariate data to be mathematically represented by a continuous algebraic polynomial. In other words, given a set of k+1 data points,

$$(x_0, y_0),\ldots,(x_j, y_j),\ldots,(x_k, y_k)$$

where no two x_j values are the same, the Lagrange polynomial is the polynomial with the smallest degree that assumes at each x_j value, a corresponding value y_j. The polynomial *L(x)* can be calculated by the equations [20],

$$L(x) := \sum_{j=0}^{k} y_j l_j(x)$$

$$l_j(x) := \prod_{\substack{0 \le m \le k \\ m \ne j}} \frac{x - x_m}{x_j - x_m},$$

where $0 \le j \le k$.

3.2 The model

The model first required the input of raw data for a single spectrum at an initial viewing angle of 10°. This data set includes simply the relative intensities for each whole number wavelength in a given interval. However, the limitations of Lagrange interpolation [21] meant that for the most accurate polynomial, the number of data points used had to be smaller than the total number of data points available (350nm to 1000nm in 1nm intervals). Therefore, only a certain section of a spectrum can be modelled to ensure the resulting polynomial accurately represents the data in the given wavelength range. Through the careful selection of data points, a modelled spectrum such as the one in figure 3.1 may be produced.

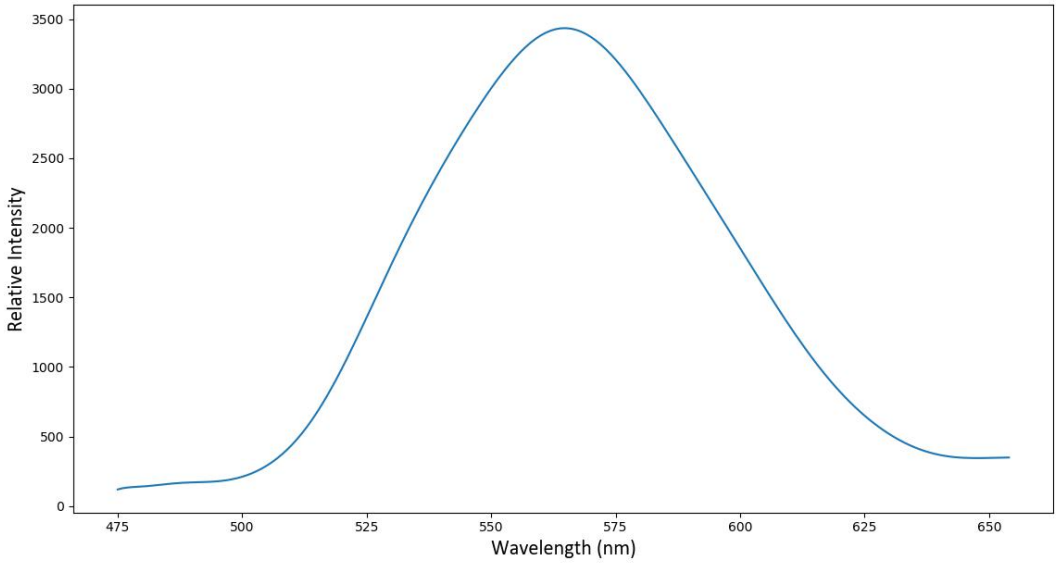

Figure 3.1: *The Lagrange polynomial L(x) for a spectrum taken at 10° in the interval 475-655nm*

The RMSD values for the polynomial and observed data are incredibly small in that they can be considered zero, therefore the polynomial fits the data perfectly.

3.2.1 Changing angle of view

To predict the spectra at different viewing angles, only the polynomial for the initial spectra is required (figure 3.1) since equations 2 and 4 describe the changes in wavelength and relative intensity respectively for the dominant reflected peak. Vertical and horizontal transformations can be applied to the polynomial L(x) to produce a new function $L_2(x)$,

$$L_2(x) = \delta I L(x + \delta\lambda),$$

where δI and δλ are multipliers calculated from equations 2 and 4 ($\delta I \leq 1$). It is considered that every point (x, L(x)) undergoes this transformation since the relative intensities for any wavelength reduce in the same manner to the dominant reflected wavelength. However, wavelengths other than the dominant reflected wavelength do not undergo a blueshift, therefore at larger angles of view when δλ is larger, the RMSD increases as non-dominant wavelengths are blue shifted.

3.2.2 The program

```
import scipy
from sympy import *
import pylab
import matplotlib.pyplot as plt

x1=475
x2=655

def Lagrange(Lx,Ly):
    y=0
    X=sympy.symbols('x')
    for k in range(len(Lx)):
        t=1
        for j in range(len(Lx)):
            if j != k:
                t=t*((X-Lx[j])/(Lx[k]-Lx[j]))
        y+=t*Ly[k]
    return y
function=str(Lagrange(lx,ly))

x=sympy.symbols('x')
derivative=Derivative(Lagrange(lx,ly),x)
gradient=derivative.doit().subs({x:wavelength (nm)})

def transformations():
    l=0
    y=0
    while l<len(difference):
        for i in lx:
            t=float(i)-float(difference[l])
            unsplit.append(t)
        l+=1
    x_transformations=[unsplit[x:x+len(lx)] for x in range(0,len(unsplit),len(lx))]
    while y<len(difference):
        def graph(equation,x_range):
            x=np.array(x_range)
            y=eval(equation)
            plt.plot(x,y)
        graph(str(float(y_difference[y])*Lagrange(x_transformations[y],ly)),range(x1,x2))
        y+=1
```

Lagrange Polynomial

Gradient at a point

Transformations

Figure 3.2: *Main section of the program*

3.3 Comparing modelled spectra to observed spectra

A group of spectra can be modelled accurately if the models describing their wavelengths and relative intensities have relatively low RMSD values (≤0.03 for intensity models).

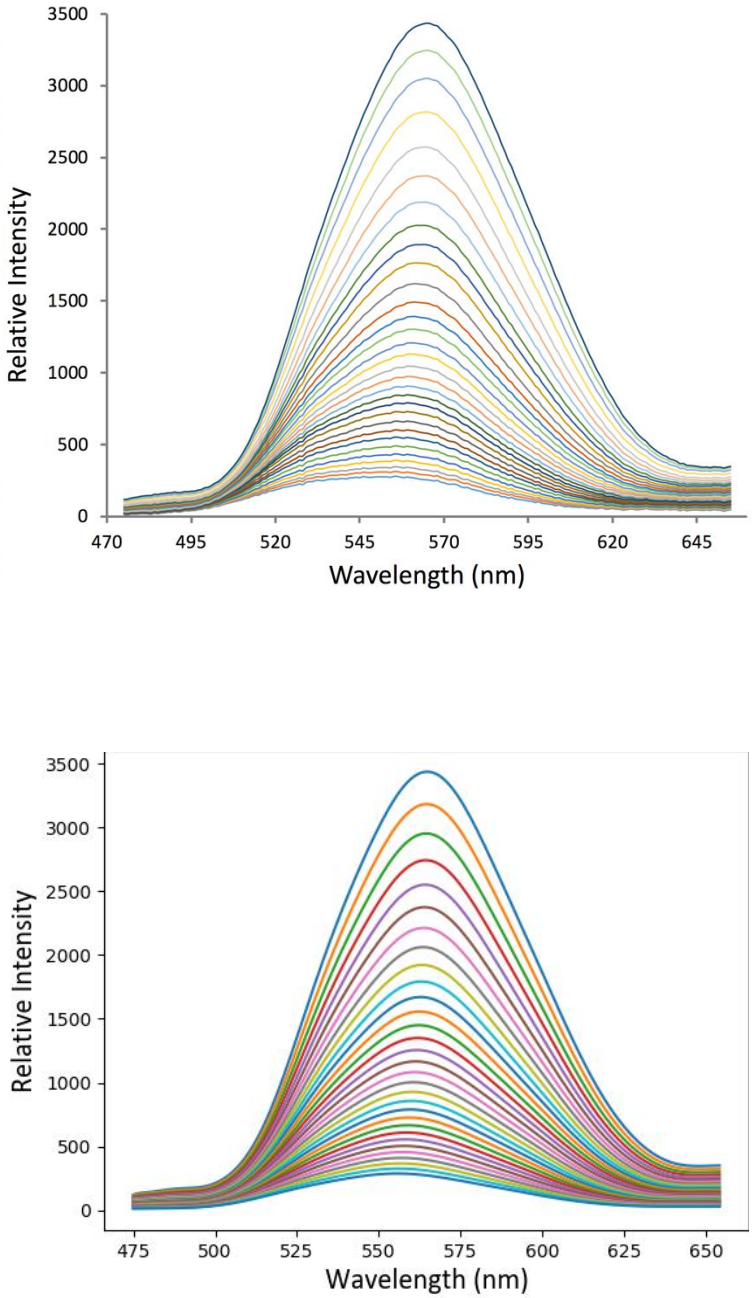

Figure 3.3: *Observed spectra (top) and predicted spectra (bottom)*

Chapter 4: Modelling Multilayer Reflectance

In this chapter, I intend to investigate how the intensity of reflected light varies with the wavelength of incident light and angle of incidence. The aim is to model reflectance using mathematical equations derived from boundary conditions set up from Maxwell's equations, including Fresnel equations and the transfer matrix method for multilayer reflectance. Before the models are addressed, a basic overview of computational electrodynamics must first be established.

4.1 Maxwell's equations

Light is an electromagnetic wave made up of oscillating magnetic and electric fields. The electric and magnetic field vectors are perpendicular to one another and the direction the wave is travelling (figure 4.1). The direction of oscillation of the electric field determines the waves polarisation.

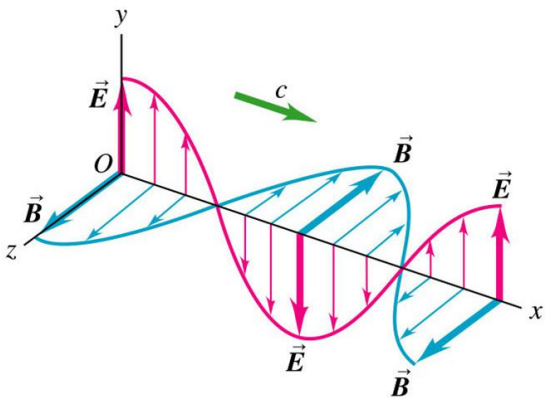

Figure 4.1: *Diagram of an electromagnetic wave [22]*

The Maxwell equations are a set of partial differential equations which provide a model for how electric and magnetic fields are generated by charges, currents and changes of the electric and magnetic fields. More importantly they describe how fluctuating magnetic and electric fields propagate at the speed of light. In the case of light waves interacting with a dielectric[7] multilayer structure, a version of Maxwell's equations are used which are named the "macroscopic" Maxwell equations. These equations describe the large-scale behaviour of matter [23]. The macroscopic Maxwell equations are shown below,

$$\nabla \cdot \mathbf{D} = \rho,$$
$$\nabla \times \mathbf{E} = -\frac{\partial \mathbf{B}}{\partial t},$$
$$\nabla \cdot \mathbf{B} = 0,$$
$$\nabla \times \mathbf{H} = \mathbf{j} + \frac{\partial \mathbf{D}}{\partial t},$$

[7] A dielectric material is a bad electrical conductor

Where *E* and *B* are the electric and the magnetic fields respectively. The displacement vector *D* is a rough measure of the response of the medium to the filed, and *H* is the analogue of *D* for the magnetic field [24].

4.1.1 Material equations

To solve the electromagnetic field for a given set of ρ and *j,* one has to solve the Maxwell's equations. However, there are four unknown vectors E, D, B and H and to solve them assumptions have to be made, and these assumptions give us the material equations,

$$\mathbf{D} = \epsilon \mathbf{E},$$
$$\mathbf{H} = \frac{1}{\mu}\mathbf{B},$$
$$\mathbf{j} = \sigma \mathbf{E}.$$

Such materials where these relations are valid are known as Linear-Isotropic-Homogenous or LIH mediums [24]. When modelling the natural multilayer reflector, the two media, chitin and air are considered to be LIH mediums.

4.2 Reflection at an interface

From chapter 1, we established the physics involved in thin film interference which considered interference of reflected waves from the upper and lower boundaries (figure 1.1). If this interface is flat and smooth, then the reflected light at both boundaries will be reflected at an angle equivalent to the initial angle of incidence (figure 2.2). The term *reflectance* refers to the *ratio of the intensity of the reflected light to the intensity of incident light at a single interface or boundary [25]*. We can derive expressions for the amount of reflection and transmission at a dielectric interface between two media, by applying boundary conditions for the electric and magnetic fields at the interface, which are known from Maxwell's equations. Specifically, the components of the electric field *E* and magnetic field *B*, which are tangent to the surface, must be continuous across the boundary [26].

4.2.3 Polarisation

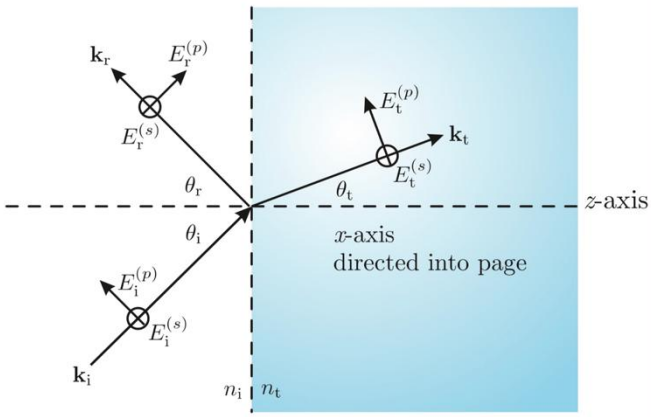

Figure 4.2: *Diagram demonstrating the different polarisation states at an interface. The superscripts "s" and "p" above the electric field E refer to the s and p polarisations respectively and the vector k is the direction of propagation [26]*

To derive expressions for reflectance, the polarisation of light with respect to the plane of incidence[8] must be taken into account. There are two cases of polarisation [27]:

- Transverse Electric (TE): Electric field perpendicular to the plane of incidence, also called s-polarisation
- Transverse Magnetic (TM): Magnetic field perpendicular to plane of incidence, also called p-polarisation

4.2.4 Fresnel coefficients

The laws of electromagnetism, applied to this case, give the following boundary conditions [27]:

1. The perpendicular component of B is continuous across the boundary between two media
2. The parallel component of E is continuous across the boundary between two media.

Using these conditions, it is possible to derive the ratio of reflected to intensity amplitudes E_r and E_i for reflected and incident light respectively. From condition 2, E is parallel to the boundary therefore,

$$E_i + E_r = E_t$$

From condition 1, the continuity of the perpendicular components of B is expressed by,

$$B_i \cos\theta_i - B_r \cos\theta_r = B_t \cos\theta_t$$

The ratio of reflected to incident amplitudes, r_s, for s-polarised light can be derived easily from these two conditions. The expression is given by,

$$r_s = \frac{E_r^{(s)}}{E_i^{(s)}} = \frac{n_i \cos\theta_i - n_t \cos\theta_t}{n_i \cos\theta_i + n_t \cos\theta_t},$$

where n_i and n_t are the refractive indices of the incident and transmitting media. For p-polarised light the ratio is given by,

$$r_p = \frac{E_r^{(p)}}{E_i^{(p)}} = \frac{n_i \cos\theta_t - n_t \cos\theta_i}{n_i \cos\theta_t + n_t \cos\theta_i}.$$

The values r_s and r_p are known as the Fresnel reflection coefficients. There are also coefficients for transmittance[9], but they will not be necessary.

4.2.5 Reflectance

[8] The plane of incidence is a plane containing the surface normal and the propagation vector

[9] Transmittance is the ratio of transmitted light to incident light.

Since intensity is proportional to the square of the amplitude of the electric field, we can write the fraction of light reflected from the surface (Reflectance) in terms of the Fresnel coefficients,

$$R_s \equiv \left|r_s\right|^2 \qquad \text{and} \qquad R_p \equiv \left|r_p\right|^2$$

These equations are known as the Fresnel equations. And for unpolarised light, the reflectance is,

$$R = \frac{R_s + R_p}{2}.$$

4.3 Reflection at multiple interfaces

So far, we have dealt with the reflection at a single dielectric interface at non-normal angles of incidence and found the ratio of reflected light depends upon the angle of incidence and the polarisation of the incident light. However, calculating the reflectance for a multilayer reflector requires different mathematics and parameters including the thickness of the individual layers.

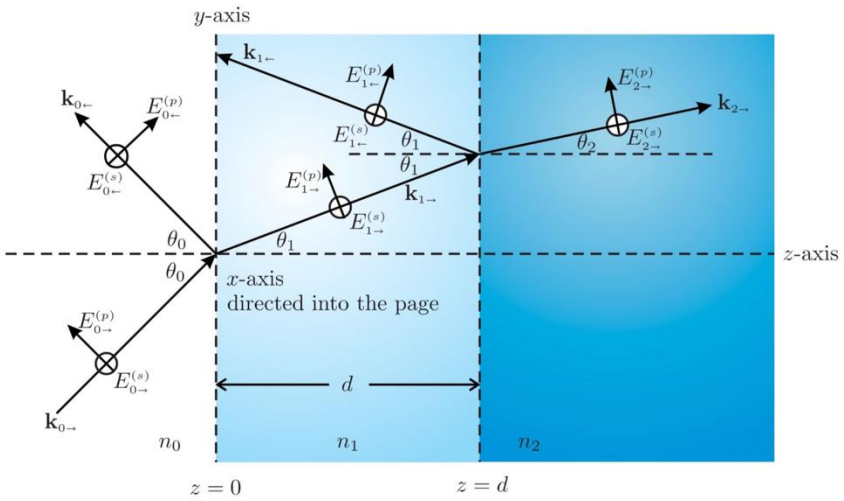

Figure 4.3: *Waves propagating through a dual interface between materials [26]*

In figure 4.3, the Electric fields have been separated into their corresponding s and p polarised components. The subscripts i, r and t have been replaced with arrows since there are multiple waves travelling in the same direction (either forwards or backwards).

4.3.1 Transfer Matrix Method

One method of calculating reflectance for a multilayer stack is called the transfer matrix method which relates the electric and magnetic fields at both interfaces of an optical element via a characteristic matrix. Larouche and Martinu [28] provide an accessible treatise that lays out the mathematics which we will be summarised here.

As shown in figure 4.4, a multilayer stack consists of multiple layers with thickness d_i and refractive indices N_i between an incident and exit media of indices of refraction N_{inc} and N_{ex} respectively.

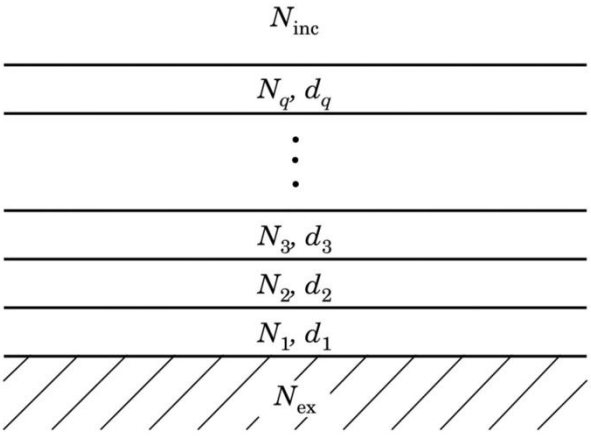

Figure 4.4: *A Multilayer stack [x]*

The i^{th} layer of a multilayer structure can be represented by the matrix,

$$M_i = \begin{bmatrix} \cos\varphi_i & (i/\eta_i)\sin\varphi_i \\ i\eta_i \sin\varphi_i & \cos\varphi_i \end{bmatrix},$$

where

$$\eta_i = \begin{cases} N_i \cos\theta_i & \text{S polarisation} \\ N_i / \cos\theta_i & \text{P polarisation} \end{cases}$$

is the pseudoindex of the layer,

$$\varphi_i = \frac{2\pi}{\lambda} N_i d_i \cos\theta_i$$

is the phase shift of the wave inside the layer, θ_i is the angle of propagation in the layer obtained from Snell's law, and λ is the wavelength of light in a vacuum. The characteristic matrix describing the multilayer is

$$M = \begin{bmatrix} m_{11} & m_{12} \\ m_{21} & m_{22} \end{bmatrix} = \prod_{i=q}^{1} M_i,$$

where q is the number of layers, and the product is taken in reverse order since the matrices of the upper layers must be multiplied on the left. The amplitude reflection coefficients of the multilayer can be calculated by,

$$r = \frac{\eta_{inc} m_{11} - \eta_{ex} m_{22} + \eta_{inc}\eta_{ex} m_{12} - m_{21}}{\eta_{inc} m_{11} + \eta_{ex} m_{22} + \eta_{inc}\eta_{ex} m_{12} + m_{21}}$$

where η_{inc} and η_{ex} are the pseudoindicies of the incidence and exit media respectively. The reflectance is calculated by,

$$R = rr^* = |r|^2$$

where * denotes the complex conjugate of the reflection coefficient since the coefficients themselves are complex numbers.

4.4 Modelling reflectance for changing θ_i

For a single interface, the Fresnel equations are ideal for modelling reflectance for any given wavelength of incident light. The first part of modelling multilayer reflectance was to simplify the multilayer system to a single LIH medium of chitin which treats the elytron as if it were just chitin and excludes any subsurface scattering a multilayer would produce. Hence, we have a single interface of air and chitin in which the reflectance at varying angles of incidence can be calculated by the Fresnel equations.

4.4.1 The program

Since we are dealing with unpolarised light in this investigation, the mean of the p and s Reflectance equations were calculated (figure 4.5).

```
import numpy as np
import matplotlib.pyplot as plt
n1=1
n2=1.56
i=10
t=90
while i<=t:
    angle.append(i)

    a=n1*np.cos(np.radians(i))-np.sqrt(n2**2-((n1**2)*(np.sin(np.radians(i)))**2))
    b=n1*np.cos(np.radians(i))+np.sqrt(n2**2-((n1**2)*(np.sin(np.radians(i)))**2))
    te=(a**2)/(b**2)
                                        Reflectance (s polarised)
    c=n2*np.cos(np.radians(i))-((n1/n2)*np.sqrt(n2**2-((n1**2)*(np.sin(np.radians(i)))**2)))
    d=n1*np.cos(np.radians(i))+((n1/n2)*np.sqrt(n2**2-((n1**2)*(np.sin(np.radians(i)))**2)))
    tm=(c**2)/(d**2)
                                        Reflectance (p polarised)
    ru=(te+tm)/2
                                        Reflectance (unpolarised)
    i+=1
```

Figure 4.5: *Main section of the program that deals with calculating reflectance*

Since the refractive index of chitin and air are known, the reflectance at an air-chitin interface can be calculated for increasing angles of incidence (figure 4.6)

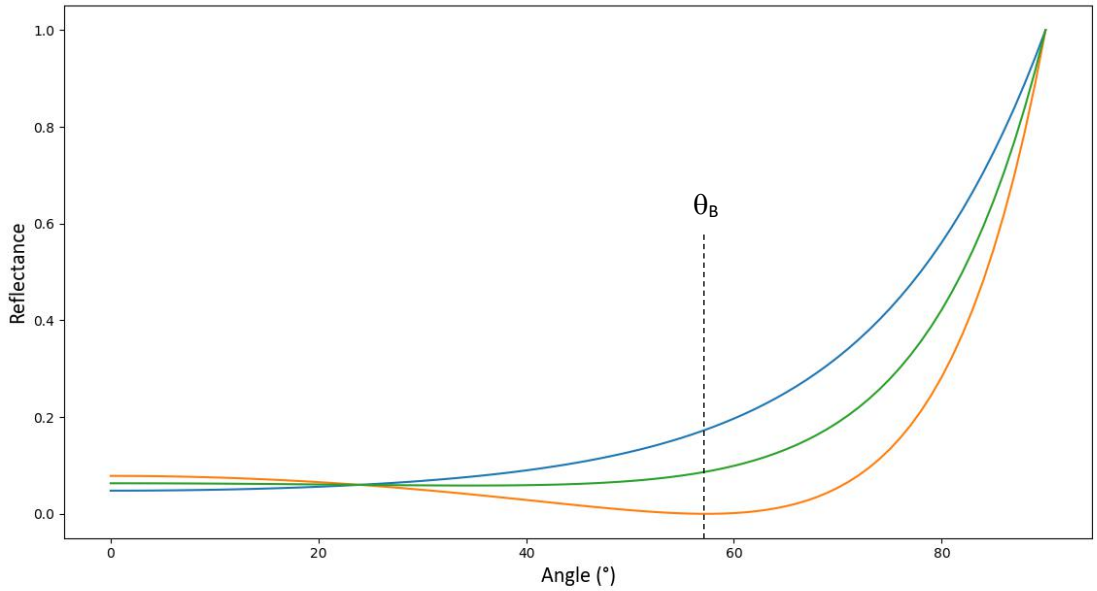

Figure 4.6: *Graph showing the reflectance for s polarised (blue), p polarised (orange) and unpolarised (green) light at an air-chitin interface from 0 °-90 ° angle of incidence.*

From figure 4.6 it is clear to see that the reflectance generally increases with increasing angle of incidence reaching 100% reflection at 90°. Furthermore, at the Brewster angle (θ_B= 57.3°) all parallel polarised light is refracted (r_p=0) meaning the reflected light is fully polarised perpendicularly to the plane of incidence [29]. Brewster's angle can be calculated by the equation,

$$\theta_B = \arctan\left(\frac{n_2}{n_1}\right).$$

4.4.2 Spectral analysis

It is important to note that that reflectance measurements were taken on much smaller and flatter elytron pieces to ensure the angle of secular reflection of reflected light is reasonably close to the angle of incidence. A total of 5 elytra were tested. Furthermore, reflection measurements were taken up to an angle of incidence of 75° because at larger angles, the relative intensity of some peaks taken beyond this angle were too large to show up in a spectrum. A typical set of reflectance spectra for a single elytron piece is shown in figure 4.7.

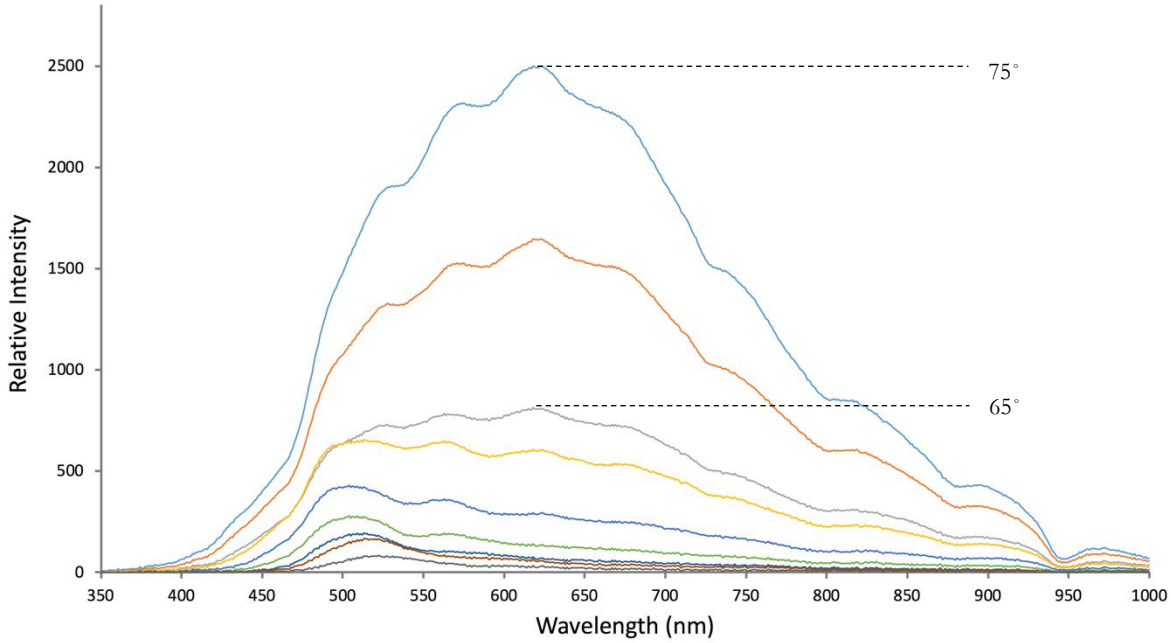

Figure 4.7: *Spectra taken from 35° -75° in 5°* intervals

From figure 4.7, it is clear too see the dominant reflection peak increases with increasing angle of incidence. As expected, the dominant reflected wavelengths blueshift from 35° to around 60° which can be modelled in a similar way to chapter 1. After 60°, the reflection peak redshifts dramatically and iridescence ceases.

4.4.3 Comparing spectral and modelled data

The graphs below consist of the reflectance (relative intensity) of the dominant reflection peaks against angle of incidence. The blue curves are modelled data.

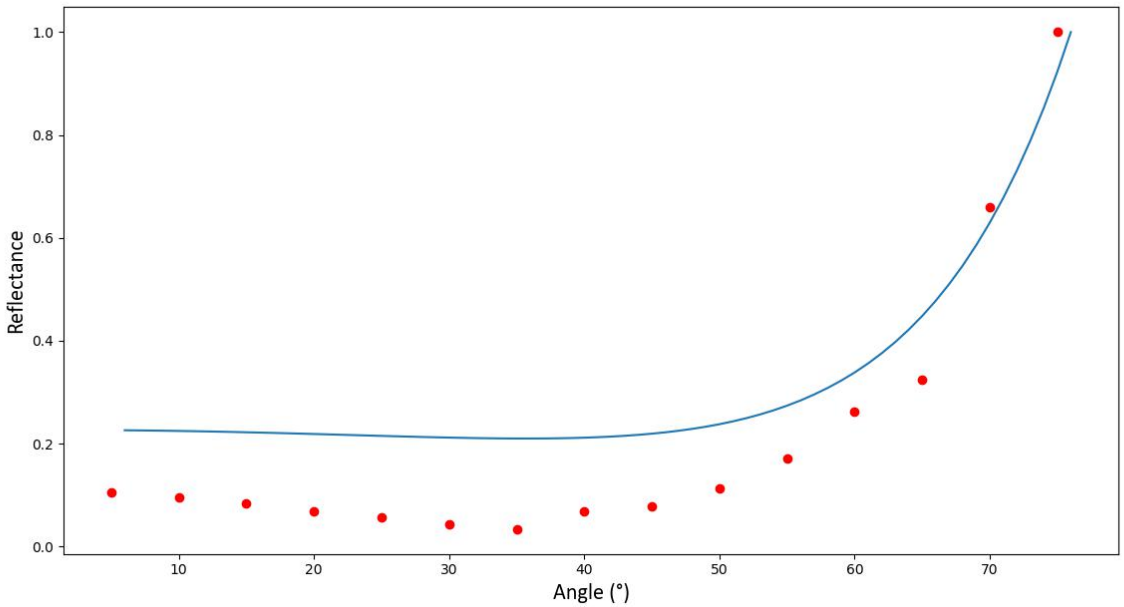

Figure 4.8

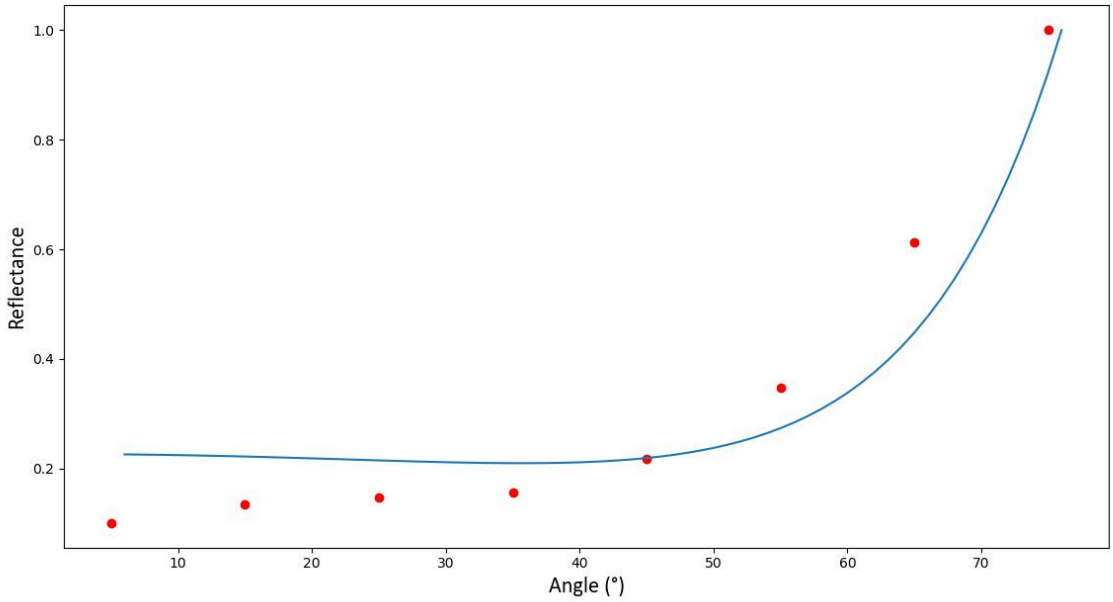

Figure 4.9

Figures 2.8 and 4.9 represent the average relationship observed between the spectral data and the model. In general, initial angles of reflectance are lower than predicted however the turning point of the modelled curve closely matches the turning point in the data at about to 50°.

4.5 Wavelength dependent reflectance

The transfer matrix method allows the reflectance of different wavelengths of incident light to be calculated, which therefore includes the conditions for constructive interference in chapter 1 which allows the position of the dominant reflection peaks to be known. Using this mathematical method, I wanted to investigate how the reflectance of different wavelengths of light change at different angles of incidence for unpolarised light using known parameters such as layer thickness and refractive index. This would allow me to explain the different features of reflectance spectra such as the ones in figure 4.7.

The parameters and conditions for the modelling of reflectance spectra are stated below:

- Alternating layers of chitin and air with refractive indices of 1.56 and 1 respectively
- Multilayer consists of 19 layers
- All layers have a thickness of 100nm (actual thickness from TEM images)
- Entrance and exit media are air and chitin respectively and are considered to be infinite
- The media are non-absorbent
- Incident light is unpolarised

A simplified version of the program is shown in figure 4.10.

Figure 4.10: *Transfer matrix calculations*

The figures below are modelled spectra produced from transfer matrices at different angles of incidence.

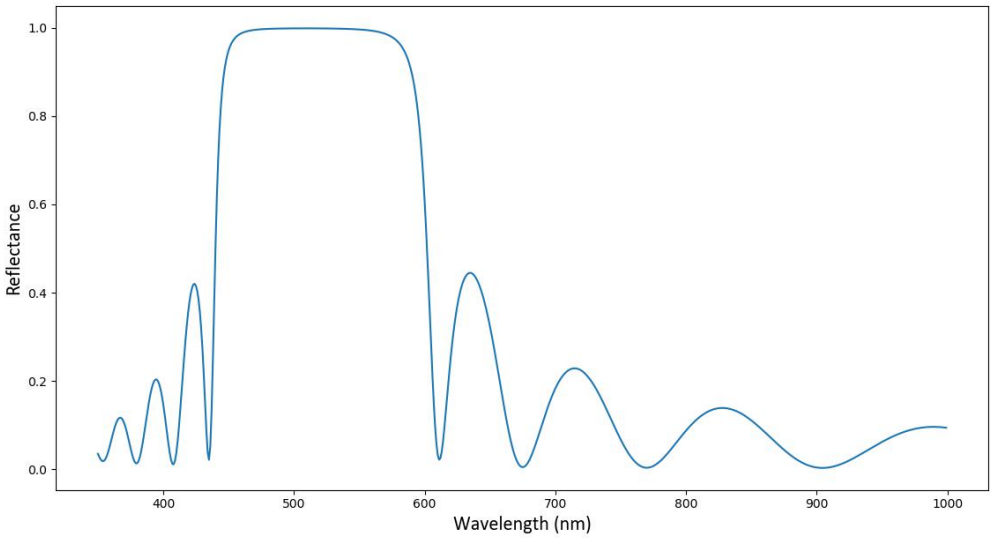

Figure 4.11: *Reflectance spectra at 10°*

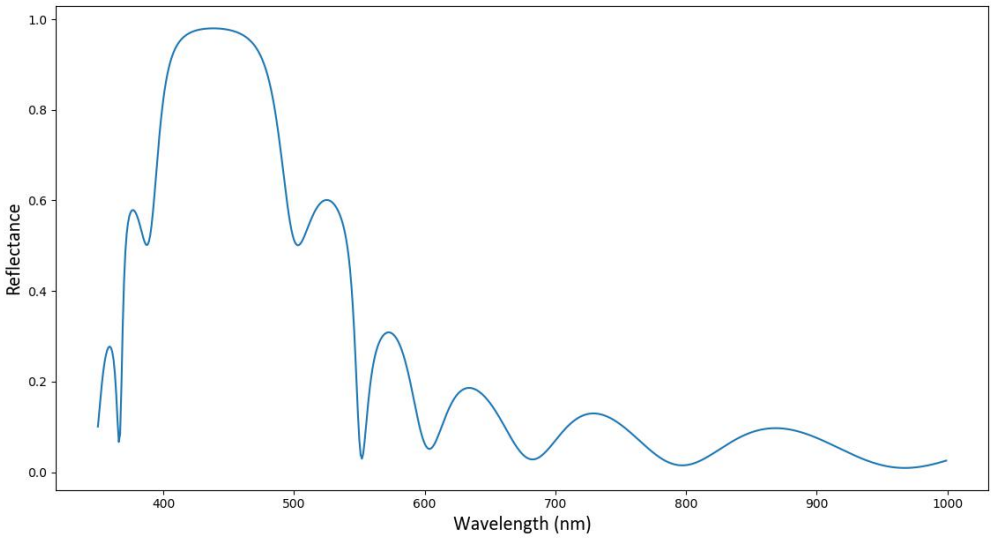

Figure 4.12: *Reflectance spectra at 40°*

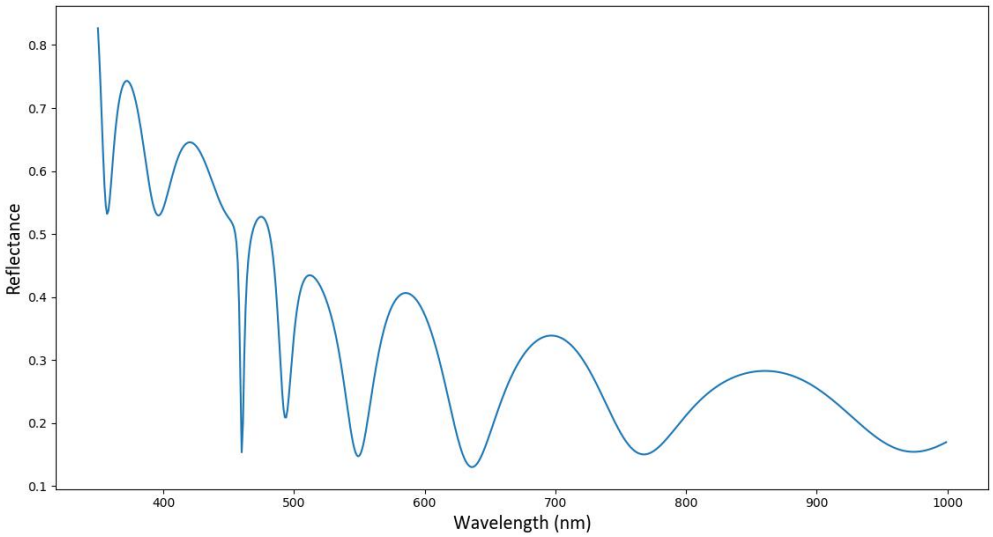

Figure 4.13: *Reflectance spectra at 75°*

From figures 4.11-4.13, it can be seen that the dominant reflected wavelength blueshifts from around 500nm at 10° to below 350nm at an angle of 75° which does not come as a surprise. However, the reflectance of smaller peaks increases relative to the dominant reflected peak as the angle of incidence increases which leads to a higher spectral bandwidth at larger angles which we will investigate in chapter 5. The graphs show that iridescence is still present at larger angles which contradicts with the spectral data obtained in figure 4.7 where the dominant reflected peak redshifted at around 60° and iridescence ceases. This result was consistent through multiple recorded reflectance spectra and my own explanation is given below:

- Since the reflectance increases with increasing angle of incidence, less incident light is transmitted through the multilayer structure. Therefore, a smaller proportion of incident light undergoes thin-film interference which will lead to the dominant reflected wavelength having a lower relative intensity relative to other reflected wavelengths. Moreover, this should mean the spectral bandwidth of a given spectrum increases with increasing angle of incidence.

This explanation has been stated here in order for the hypothesis on spectral bandwidth to make sense. A more detailed explanation involving the models is provided in the conclusion.

Chapter 5: Investigating Spectral Bandwidth

5.1 Hypothesis

Spectral Bandwidth is defined as the width of the band of light at one-half the maximum [30] peak as shown in figure 5.1.

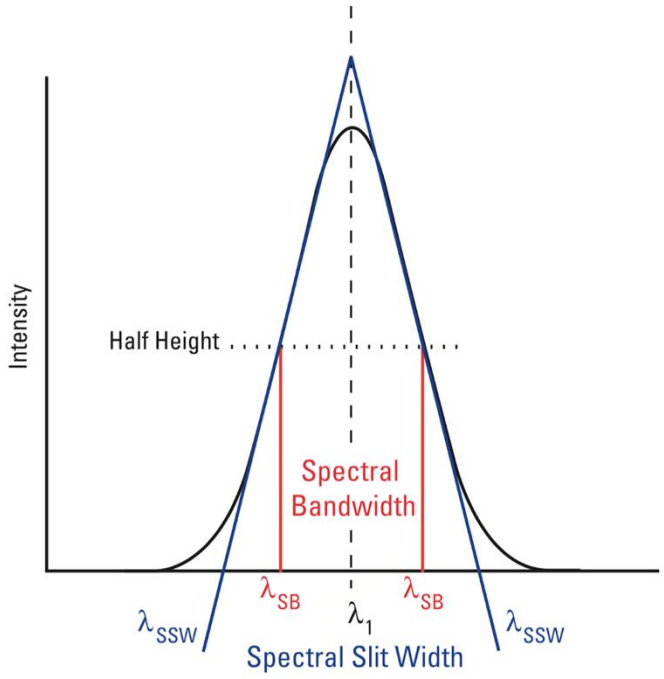

Figure 5.1: *Diagram of spectral bandwidth [30]*

From figure 5.1, the spectral bandwidth is therefore calculated by subtracting the two separate values for λ_{SB}. Spectral bandwidth was investigated as it showed to be an important characteristic in the reflectance spectra obtained from multiple elytra. The hypothesis I came up with relates

the values of reflectance and spectral bandwidth which is based off the explanation established in the previous chapter. The hypothesis is stated below:

The normalised value of reflectance is equal to the normalised value of spectral bandwidth at a given angle of incidence.

This hypothesis can be written as a simple relationship,

$$\frac{R_\theta}{R_{\max}} = \frac{\phi_\theta}{\phi_{\max}},$$

where I have denoted spectral bandwidth as ϕ. The hypothesis assumes the maximum values of reflectance and spectral bandwidth are taken at the same angle of incidence.

5.2 Comparing spectral and modelled data

To test my hypothesis, I used the model of reflectance at a single dielectric interface using the Fresnel equations. The figures below show the recorded normalised spectral bandwidth and the modelled reflectance curve (blue line).

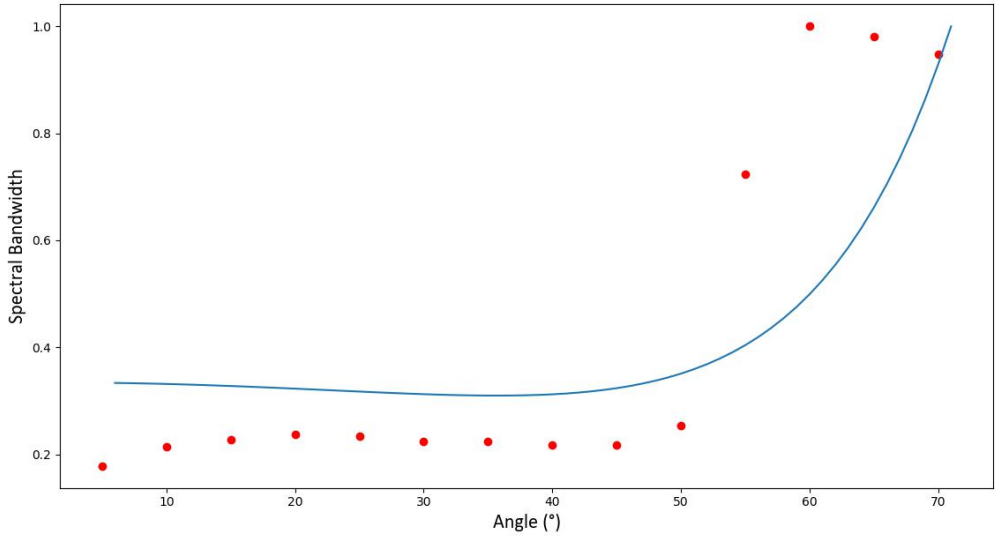

Figure 5.2

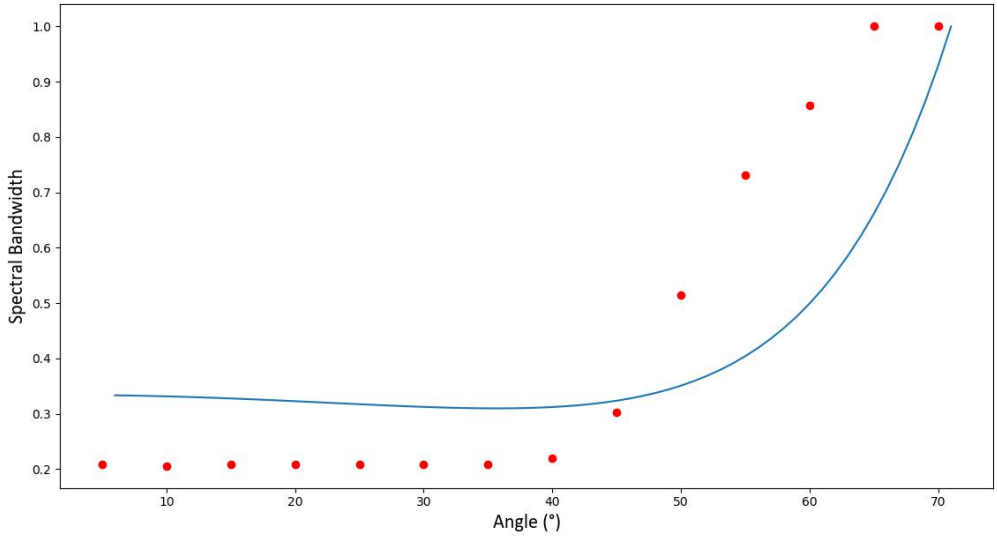

Figure 5.3

In general, it can be seen from the figures above that the spectral bandwidth increases with increasing angle of incidence which agrees with my hypothesis. However, the data values do not exactly match the predicted values as shown by the RMSD values of 0.190 and 0.173 for figures 5.2 and 5.3 respectively. Although these values are small, which imply the model predicts the change in spectral bandwidth reasonably well, they are not enough to conclude my hypothesis as being correct.

6 Conclusion

The following are conclusions I have come to regarding both spectral data and the mathematical models which are exclusive to the *C. wallacei* species.

6.1 Iridescence and the multilayer structure

6.1.1 Spectral data

From numerous experiments done on different *C. wallacei* elytra, it was confirmed that the species produces a strong green hue at angles close to normal incidence. It was found that the dominant reflected wavelength at the initial angle of incidence would vary between each specimen in the interval of about 550-570nm with the average value recorded lying close to the mean in the given interval. This variation is mostly likely due to two factors:

- *Variations in the thickness of the layers in the multilayer structure:* As the TEM images showed, the thickness of the layers were between 80-100nm with the average thickness being 100nm. This variation will cause different wavelengths of light to be reflected for different elytra since the equation for constructive interference involves the layer thickness. Furthermore, the average value of 100nm means the layers in a single multilayer stack also vary and are not perfectly alike which will also have the same effects on the dominant reflected wavelength.
- *Curved elytron surface:* The surfaces of most elytra were curved which will change the local angle of incidence at a single point on the surface therefore reflecting an unexpected wavelength of light. However, the variation of wavelength due to this factor is small which is most likely due to the large field of incident light on the surface of the elytron (0.5cm) which minimises the effects of curvature and therefore local angles of incidence.

6.1.2 The model

Overall it was clear to see through multiple comparisons that my mathematical model for iridescence I created which involved the constant k clearly predicted the trends in blueshift for multiple spectra very well as shown by the very small RMSD values. However, the difference in blueshifts for spectral data collected and the mathematical model *without* the constant k were very large. The predicted amount of blueshift the reflected wavelengths would undergo depend on the refractive indices of the layers in the stack and the predicted value for layer thickness which is in itself determined by the refractive indices.

Therefore, the main reason the data shows smaller blueshifts than expected would be the variation and uncertainty in the two values of refractive index for each medium which make up the multilayer reflector. The first medium is known definitely to be chitin or a combination of chitin and melanin which have an average refractive index of 1.56 in multiple beetle species [1-6]. It is possible that the *C. wallacei* has a higher refractive index for the chitin layer although the

difference would only be small. The second medium was considered to be air (or at least mostly air). Therefore, I conclude that the second air layer most probably includes chitin in it as well but not entirely, since the results of water treatment implied otherwise (7.2). Furthermore, similar papers to mine have established air is the second medium in multiple beetle species. In addition, it is important to note that the mathematical model could work well for a different combination of refractive indices which would give the same initial wavelengths of colour but perhaps different predicted values of layer thickness.

6.1.2.2 Predicted value of layer thickness

The average predicted value of layer thickness was obtained through several experiments and was shown to be 100nm (10nm higher than the actual average value). This difference could be due to the uncertainty or variation in refractive index, however a difference of 10nm isn't too large which implies the refractive indices used in the model aren't far off the real values (treating the natural multilayer as having uniform layer thickness).

6.2 Water treatment

The results of water treatment showed the dominant reflected peak redshifted substantially as well as other wavelengths which is what was expected. This was the case for 4 water treated elytra. This redshift in reflected colour implies that the multilayer structure does indeed have layers of air or at least pockets of air since the water clearly diffused through the pores in the surface of the elytron. Therefore, this result agrees with the fact that the layers, other than the chitin layers, in the multilayer structure do indeed contain regions of air. However, it is not known for certain that the water diffused through all the layers.

6.2.1 The model

The model predicted the water treated elytra do produce a spectrum with a smaller blueshift in dominant reflected wavelength compared to elytra before treatment, however experiments showed the opposite in which the blueshift was larger than the blueshift before treatment. This is a very intriguing result and is most likely due factors such as very small quantities of water left behind on the surface of the elytra or it could possibly be due to something more complex.

6.2.1.1 Predicted value of layer thickness

The model for water treated elytra produced smaller numbers for the layer thickness. It predicted an average of 105 nm, which is the average between the predicted value for non-treated elytra and the actual observed layer thickness. Water treatment supposedly allows the refractive index of both media in the multilayer to be known for certain in an ideal case. The predicted layer thicknesses for water treated elytra were closer to the known thickness, and this correlates well with the fact that the second media in the multilayer is air. A likely explanation for this is because the air in the non-chitin layers is replaced by water which has a known refractive index therefore the model will predict a layer thickness closer to 100nm. In addition, since the predicted thickness wasn't 100nm implies that the non-chitin layers consist of other materials other than air (most likely chitin or melanin) which the water could not physically replace in the multilayer. Therefore, a better value for the refractive index of the second media in the multilayer reflector would be the average refractive index of chitin and air which is 1.28. Using this value instead of the refractive index of air for the second media would have meant the model for iridescence matched closer with the spectral data when $k=1$.

6.3 Relative intensities

The model for relative intensity was based off my own mathematics and geometrical modelling of the elytron surface. There are many reasons why the model may not accurately predict the relative intensity of reflected light for surfaces with varying curvature. Some of the reasons are stated below:

- *The elytron cross section isn't a perfect cosine function:* The natural curvature of an elytron will never follow a perfect curve described by a cosine function.
- The main limitation for the model is that it does not take into account small irregularities and undulations on the surface of the elytron which are important to model in order to achieve an accurate reflection model.
- Does not follow the normal mathematical methods found in diffuse reflection models.

The intensity model was shown to be accurate at predicting changes in intensity for multiple elytra and was very useful in predicting spectral curves at varying angles of view.

6.4 Predicting spectral curvature

Lagrange interpolation proved to be a suitable method in accurately curve fitting a spectrum when the correct number of data points are used. However, trying to predict how a spectrum changes with varying angle of view was harder to model accurately since not all wavelengths of reflected light will undergo blueshift. Due to thin-film interference, only the dominant reflected wavelength undergoes a blueshift (and perhaps wavelengths close to the dominant wavelength). I therefore conclude that the model works well in approximating spectral curvature at varying angles, especially for wavelengths close to and including the dominant reflected wavelength. As this is the case, gradients of spectral curves can be approximated as shown in figure 3.2.

Furthermore, using all the mathematical models from chapters 1, 2 and 3 it is possible to predict the spectra for any *C. wallacei* elytron piece at any angle of incidence given that the conditions below are met:

- Spectral data of an initial spectrum at 10° (minimum viewing angle) is obtained.
- The dominant reflected wavelength at the minimum and maximum angles of view are known.
- The average maximum height and width of the cross section of the elytron are known at the point on the surface of the measurement.

6.5 Multilayer Reflectance

6.5.1 Modelling angle dependent reflectance

The reflectance models were shown to predict the data collected from flat elytron surfaces well as shown by small RMSD values. However, the differences between observed and modelled reflectance are most likely due to factors stated below:

- *The elytron surface may not be completely flat or smooth:* This is the main limitation of the modelling, since the Fresnel equations assume the interface is perfectly smooth and flat and the law of reflection is obeyed.

- *Uncertainties in multilayer parameters:* Similar to the wavelength models, uncertainties in refractive index of the layers will have a large effect on predicted reflectance.

6.5.2 Modelling wavelength dependent reflectance

From the transfer matrix method, it can be concluded that the dominant reflected wavelengths blueshift with increasing angle of incidence. In addition, the reflectance of non-dominant reflected wavelengths increases relative to the dominant wavelength reflection peak with increasing angle of incidence. My own theory to why this is stated below:

- Since the reflectance increases with increasing angle of incidence, less incident light is transmitted through the multilayer structure. Therefore, a smaller proportion of incident light undergoes thin-film interference which will lead to the dominant reflected wavelength having a lower relative intensity relative to other reflected wavelengths. Moreover, this should mean the spectral bandwidth of a given spectrum increases with increasing angle of incidence.

The point at which the blueshift of dominant reflected wavelengths cease theoretically occurs at 90°, as calculated by the model. On the other hand, the spectral data obtained showed this point occurs at around 60° for several elytra. This difference may be due to:

- Elytron surfaces not being completely smooth or flat

6.6 Spectral Bandwidth

My hypothesis stated that *"The normalised value of reflectance is equal to the normalised value of spectral bandwidth at a given angle of incidence"*. It was observed that the spectral bandwidth does indeed increase with increasing angle of incidence, however, the values of normalised reflectance did not exactly match that of the normalised values of spectral band width. Therefore, I cannot conclude my hypothesis is completely true, and more experimental data would need to be collected to ensure a valid conclusion. However, if we assume my hypothesis is correct, then some of the limitations of the modelling are stated in 6.5.

7 Evaluation

I achieved the aim I set out with, as I modelled very successfully the different optical aspects of the elytra of *C. wallacei* beetles using advanced mathematics, I taught myself, and my own modelling. The investigation of water treatment and mathematical modelling as a whole of *C. wallacei* elytra is the first of its kind as far as I'm aware, and the multilayer reflector of the *C. wallacei* has not been studied until now. My original mathematical models I designed myself were:

- Equation for constructive interference of a multilayer involving a constant k
- Relative intensity model
- Predicting spectral curvature
- Application of the Fresnel equations to model reflectance

The idea of predicting spectral curvature at any angle of view has not been attempted before and my model for relative intensities is completely unique. In addition, my hypothesis on spectral bandwidth appears to be unique as well, especially for the *C. wallacei* elytra. Although my models do indicate high accuracy in predicting data, I would need to collect more data to be more certain that it is indeed the case, especially for water treatment as only 4 elytra were treated. With the

research I have conducted over the last year and the models I have produced, I like would to investigate the optical properties of other species of iridescent beetles to see if the mathematical models can be used as effectively as they were for the *C. wallacei*. I would go about this in a similar process in that TEM images of the elytra would have to be taken beforehand. In addition, to give a complete conclusion on the accuracy of my models, a manufactured multilayer with exact known parameters and dimensions could replace a beetle elytron. That way, the mathematical models will most likely be better at predicting spectral data and can be tested with high levels of certainty.

My research and mathematical modelling could well have important applications in thin-film technology such as solar panels, digital cameras and anti-reflection coatings. Furthermore, my research has broadened the understanding of naturally occurring photonic crystals. This project has also broadened my knowledge of different areas of physics, especially optics. I now have substantial knowledge and experience of multilayer reflectors in iridescent beetles and also my mathematical and coding skills have also been improved and expanded on as a result. This is very useful as I plan to embark on a career involving mathematical physics, in which the advanced undergraduate mathematics and optical theories I have learnt now will seem easier when I come across them later in my career. In addition, other key skills I learnt include data analysis in Excel which I was inexperienced with previously. I now know how to effectively handle and analyse large data sets which may be very useful later in my physics career. This project also gave me the fantastic opportunity to use methods such as transmission electron microscopy which is very unusual for people and my position to be able to take advantage of. This imaging technique proved to be vital in the mathematical modelling.

Acknowledgments

There are certain individuals I would like to show my appreciation to for their great help with my project:

- Ilya Carey, for the support and organisation in the Beetles project at my school.
- Dr B. Kirby, for running the Beetles project and her help with my project such as providing me with academic papers.
- Ayesha Wilson and Ian Brown for organising and allowing me to use their electron microscope at the University of Kent

Images of C. wallacei elytra

Figure a: *Two non-treated elytra*

Figure b: *Water treated elytron*

References

[1] M.F Land "The Physics and Biology of Animal Reflectors", Department of Physiology-Anatomy, University of California, Berkeley. [accessed 15 October 2017]

[2] Doekele G. Stavenga, Bodo D. Wilts, Hein L. Leertouwer, and Takahiko Hariyama "Polarized iridescence of the multilayered elytra of the Japanese jewel beetle, Chrysochroa fulgidissima" [accessed 1 February 2018]

[3] J.A. Noyes, P.Vukusic and I.R Hooper "Experimental method for reliably establishing the refractive index of buprestid beetle exocuticle" School of physics, The University of Exeter [accessed 2 January 2018]

[4] T.M Jordan, J.C Partridge and N.W. Roberts "Disordered animal multilayer reflectors and the localization of light" [accessed 2 January 2018]

[5] Review article, science wise publishing, Tim Starkey and Pete Vukusic "Light manipulation principles in biological photonic systems" 2013, Nanophotonics Review [accessed 13 December 2017]

[6] Shinya Yoshioka and Shuichi Kinoshita "Direct determination of the refractive index of natural multilayer systems" [accessed 8 January 2018]

[7] Wikipedia, Iridescence, 2018: https://en.wikipedia.org/wiki/Iridescence [accessed 11 April 2018]

[8] Wikipedia, Thin Film Interference, 2018: https://en.wikipedia.org/wiki/Thin-film_interference [accessed 11 April 2018]

[9] Justin Peatross and Michael Ware, Brigham Young University August 14, 2008 "Physics of Light and optics" [accessed 14 March 2018]

[10] https://physicsthings.wordpress.com/as-physics/unit-2-mechanics-materials-and-waves/phase-difference-and-path-difference-2/ [accessed 20 May 2018]

[11] http://rsif.royalsocietypublishing.org/content/10/87/20130394 [accessed 1 May 2018]

[12] http://www.oceanopticsbook.info [accessed 15 Feb 2018]

[13] Deparis, "Structurally tuned iridescent surfaces inspired by nature": http://iopscience.iop.org/article/10.1088/1367-2630/10/1/013032/meta;jsessionid=BE2C9E47E4090DFD7A1AE69D8360AE9F.c1.iopscience.cld.iop.org [accessed 12 May 2018]

[14] Wikipedia, Radiant Intensity: https://en.wikipedia.org/wiki/Radiant_intensity [accessed 17 March 2018]

[15] Wikipedia, Radiance: https://en.wikipedia.org/wiki/Radiance [accessed 17 March]

[16] Wikipedia, Inverse Square Law: https://en.wikipedia.org/wiki/Inverse-square_law [accessed 17 March]

[17] Azooptics, Specular Reflection: https://www.azooptics.com/Article.aspx?ArticleID=822 [accessed 19 March 2018]

[18] Wolfram Mathworld, elliptic integral of the third kind: http://mathworld.wolfram.com/EllipticIntegraloftheThirdKind.html [accessed 15 March 2018]

[19] M Oren and S.K. Nayer: "Diffuse Reflectance from Rough Surfaces" [accessed 4 June 2018]

[20] Wikipedia, Lagrange Polynomial: https://en.wikipedia.org/wiki/Lagrange_polynomial [accessed 12 March]

[21] Jim Lambers, Lecture 5 notes: http://www.math.usm.edu/lambers/mat772/fall10/lecture5.pdf [accessed 13 March 2-18]

[22] Mini physics, Electromagnetic wave diagram: https://www.miniphysics.com/uy1-electromagnetic-spectrum-sinusoidal-em-plane-waves.html

[23] Wikipedia, Maxwell's Equations: https://en.wikipedia.org/wiki/Maxwell%27s_equations [accessed 16 June 2018]

[24] J.D. Jackson, "Maxwell's equations and material equations" [accessed 20 June 2018]

[25] Wikipedia, Reflectance: https://en.wikipedia.org/wiki/Reflectance [accessed 21 June 2018]

[26] Textbook, Justin Peatross and Michael Ware, "Physics of Light and Optics" [accessed 10 December 2017]

[27] Physics 263, Deriving the Fresnel equations (PDF) http://physics.gmu.edu/~ellswort/p263/feqn.pdf [accessed 22 June 2018]

[28] S. Larouche and L. Martinu, "OpenFilters: open-source software for the design, optimization, and synthesis of optical filters" [accessed 12 January 2018]

[29] Wikipedia, Brewster's angle, https://en.wikipedia.org/wiki/Brewster%27s_angle [accessed 29 June 2018]

[30] Nicole Keppy - Thermo scientific, "Understanding Spectral Bandwidth and Resolution in the Regulated Laboratory". [accessed 7 April 2018]